iScience

CellPress
OPEN ACCESS

Article

Time-restricted feeding entrains long-term behavioral changes through the IGF2-KCC2 pathway

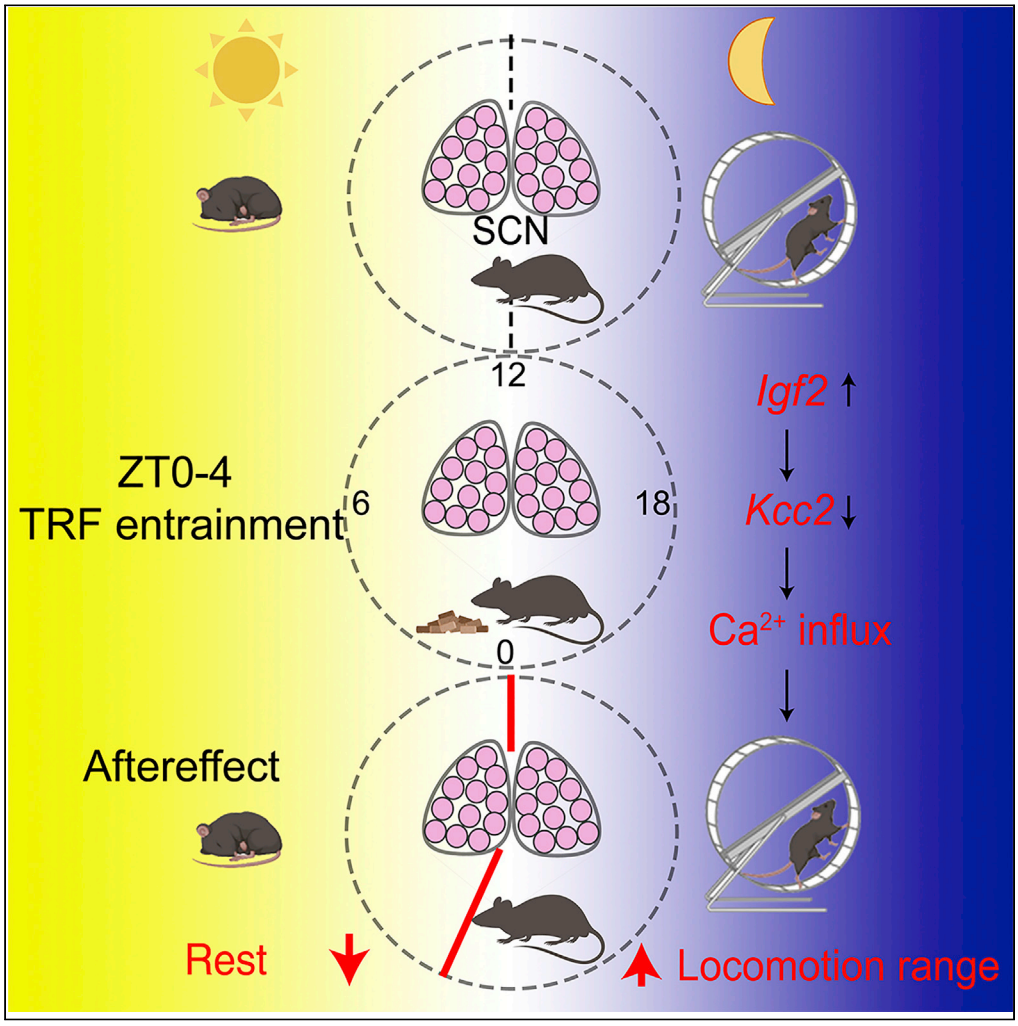

Qiaocheng Zhai, Yizhun Zeng, Yue Gu, ..., Xiaowei Chen, Antonio Vidal-Puig, Ying Xu

yingxu@suda.edu.cn

Highlights

Time-restricted feeding near light-on induces long-term behavioral changes

The suprachiasmatic nucleus (SCN) neurons can be activated by TRF stimulation

The IGF2-KCC2 pathway is associated with behavioral response to TRF entrainment

Zhai et al., iScience 25, 104267
May 20, 2022
https://doi.org/10.1016/j.isci.2022.104267

iScience

CellPress
OPEN ACCESS

Article

Time-restricted feeding entrains long-term behavioral changes through the IGF2-KCC2 pathway

Qiaocheng Zhai,[1] Yizhun Zeng,[1] Yue Gu,[1] Zhihao Li,[1] Tao Zhang,[1] Baoshi Yuan,[1] Tao Wang,[1] Jie Yan,[2] Han Qin,[3] Ling Yang,[2] Xiaowei Chen,[3] Antonio Vidal-Puig,[4,5] and Ying Xu[1,6,*]

SUMMARY

The suprachiasmatic nucleus (SCN) integrates light and systemic signals from peripheral tissues to coordinate physiology and behavior daily rhythms. However, the contribution that nutrients and feeding patterns provide to the SCN network regulation remains controversial. Here, we found that time-restricted feeding (TRF) in ZT0-4 (Zeitgeber Time) generates a robust and long-term shift in locomotor behavior and increased wakefulness. Intracellular Ca^{2+} signals in SCN GABAergic neurons of freely moving mice showed significant activation after ZT0-4 TRF treatment. Furthermore, RNA-seq profiling of SCN showed that TRF during ZT0-4 increased Insulin-like Growth Factor 2 (*Igf2*) expression and dysregulated ion transporters, including the downregulation of *Kcc2*. SCN neuron-specific loss of function of *Kcc2* amplified ZT0-4 TRF induced aftereffect. Moreover, overexpression of IGF2 in SCN GABAergic neurons extended the locomotion range, mirroring the TRF aftereffect. In summary, our study showed that the IGF2-KCC2 pathway plays an important role for TRF induced behavior changes.

INTRODUCTION

Circadian rhythms are approximately 24-h cycles in physiology and behavior. The suprachiasmatic nucleus (SCN) is the central circadian pacemaker in mammals that can be entrained by photic and nonphotic information to allow their physiologic and behavioral period to match that of an environmental oscillation (Challet, 2019; Herzog et al., 2017; Kuhlman, 2007; Welsh et al., 2010). In addition, the SCN can adjust the onset and offset of activity depending on the photoperiod length, and such adjustments can persist under constant darkness (DD), suggesting that the SCN can be entrained by seasonal changes (Farajnia et al., 2014; Houben et al., 2009; Inagaki et al., 2007; Kon et al., 2014; Olde Engberink et al., 2018, 2020; Schaap et al., 2003; VanderLeest et al., 2007). Light, the most potent natural zeitgeber or timing cue, can entrain SCN to lead physiological and behavioral processes to adapt to the external light/dark cycle.

In contrast to light, food intake availability is one of several nonphotic periodic signals shown to entrain active metabolic tissues (Challet, 2019; Mistlberger, 2011; Reinke and Asher, 2019), but it remains uncertain at the level of the SCN. Specific feeding patterns following either a typical pattern of daytime eating for diurnal animals or nighttime eating for nocturnal animals have distinctive effects on metabolic homeostasis (Fonken and Nelson, 2014; Kelly et al., 2020; Liu et al., 2014). A very recent study showed that 5 g of chocolate feeding (rat daily food consumption of approximately 15–20 g) at the onset of the active phase prevented circadian disorder from a jet-lag schedule accompanied by an increase in the amplitude of the day-night c-Fos activation in the SCN (Escobar et al., 2020), suggesting that feeding appears to be a Zeitgeber, not only in metabolically active tissues but also in the SCN. If a mistimed feeding (that is, when feeding occurs during an unusual time) is capable of acting as a zeitgeber in the SCN neurons and thereby modulate the output of SCN function, we would need to rethink the consequence of time-restricted feeding on metabolic health, sleep disorders and immune function.

Previous studies have also shown that restricted daytime feeding increases vasopressin release from the rat SCN (Andrade et al., 2004) and resets the circadian clock in the SCN of white-footed mice and inbred CS strain house mice (Abe et al., 2007). On the other hand, the observation that mice exposed to 4-h time-restricted feeding (TRF) at a relatively low temperature (21°C)die but that SCN lesions rescue this

[1]Jiangsu Key Laboratory of Neuropsychiatric Diseases and Cambridge-Su Genomic Resource Center, Medical School of Soochow University, Suzhou, Jiangsu 215123, China

[2]School of Mathematical Sciences, Soochow University, Suzhou 215006, P. R. China

[3]Brain Research Center and State Key Laboratory of Trauma, Burns, and Combined Injury, Third Military Medical University, Chongqing 400038, China

[4]University of Cambridge Metabolic Research Laboratories, Institute of Metabolic Science, MDU MRC, Cambridge, UK

[5]Cambridge University Nanjing Centre of Technology and Innovation, Jiangbei Area, Nanjing, P.R. of China

[6]Lead contact

*Correspondence: yingxu@suda.edu.cn

https://doi.org/10.1016/j.isci.2022.104267

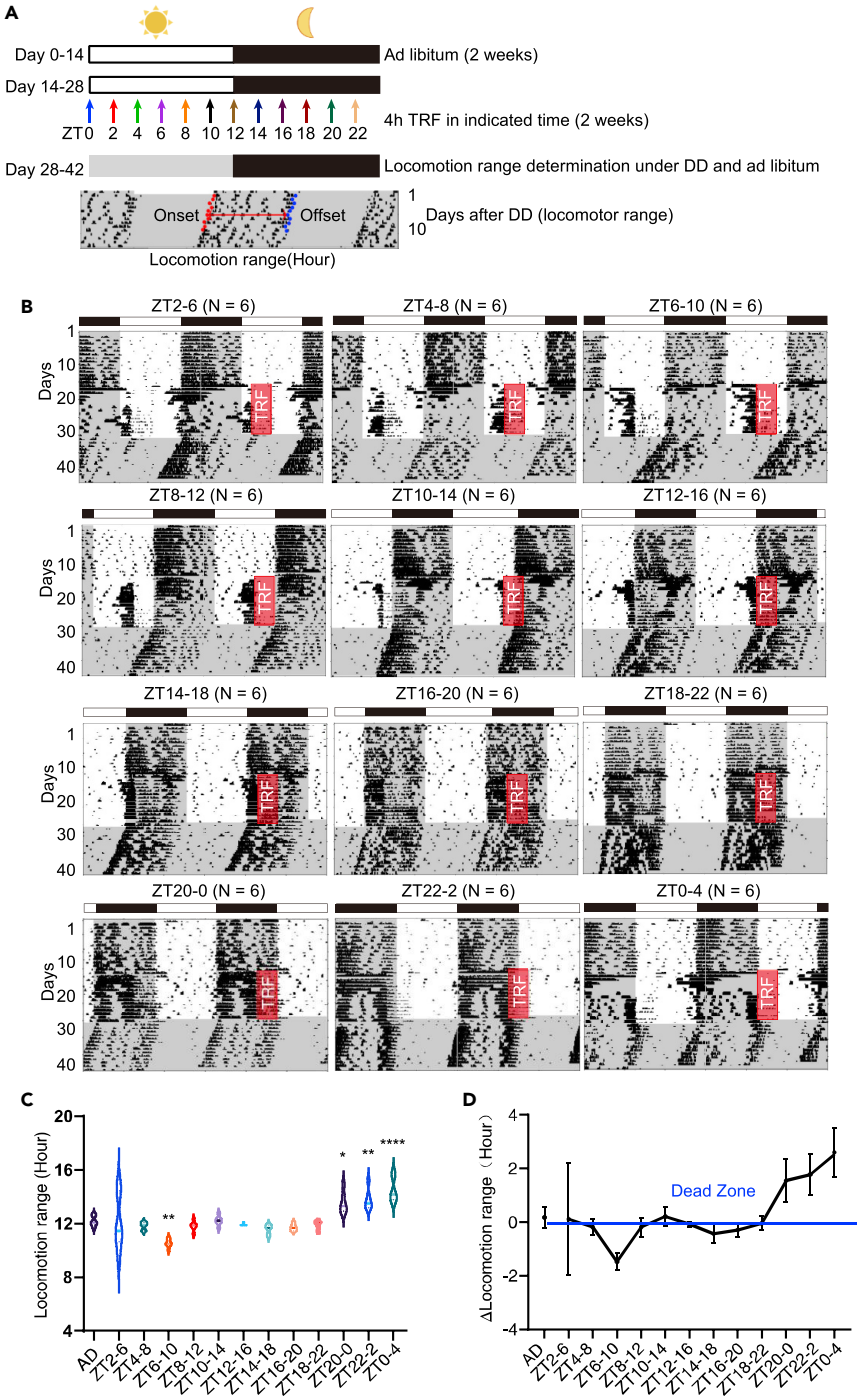

Figure 1. The effect of TRF on mouse locomotion

(A) Experimental design for time-restricted feeding. The animals were first entrained under 12 h:12 h light-dark cycles for 2 weeks. Then, 4-h TRF at 12 different phases (colored arrows) was introduced for 2 weeks. Finally, the animals were released to AD and constant darkness for 2 weeks to evaluate the locomotion changes. The red and blue dots represent locomotion onset and offset respectively. The locomotor range is calculated as the average time between onset and offset of locomotor activity for a total of 10 successive days (thereafter, except indicated) after release to *ad libitum* under constant darkness.

Figure 1. *Continued*

(B) Representative actogram of the TRF at 12 different phases (ZT2-6, ZT4-8, ZT6-10, ZT8-12, ZT10-14, ZT12-16, ZT14-18, ZT16-20, ZT18-22, ZT20-24, ZT22-2 and ZT0-4, n = 6). Red rectangle: TRF window. The gray area represents the dark phase. The number of mice at each time point is indicated at the top of the graph thereafter.

(C) The locomotion ranges of 12 phases of TRF entrainment including *ad libitum* as control mice (n = 6).

(D) The phase-response curve by the TRF entrainment. The locomotion ranges were subtracted by 12 h correspond to the TRF time. Values represent the average ±SD, *: $p < 0.05$, **: $p < 0.01$, ****: $p < 0.0001$. All p values are from two-tailed Student's *t*-tests. See also Figure S1.

phenotype (Zhang et al., 2020), supports the idea that the SCN might react to TRF-induced hunger. Notably, cyclic adenosine monophosphate (cAMP) has been reported to modulate neuronal excitability in the SCN and is an integral component of the SCN regulating transcriptional cycles (Hastings et al., 2019; O'Neill et al., 2008). In addition, dynamic regulation of SCN excitability is tied to the redox state through nontranscriptional modulation of multiple potassium (K^+) channels (Wang et al., 2012). These results offer multiple intermingled possibilities by which feeding cues can affect the inputs to modulate the outputs of the SCN. Therefore, even if a transcriptional-translational negative feedback loop (TTFL) in the SCN may not be reset by food availability, the various cross talks between ion channels, neuropeptides, and metabolic pathways occurs in the SCN that may reach all organs and cells in the body in response to TRF. Because of the prevalence of improper mealtime in the modern society, studying the entrainment of the SCN by feeding time is valuable for understanding not only the basic mechanism but also the etiology of clock-related diseases.

In the present study, we conducted unbiased screening to identify nonphotic entrained behavioral effect(s) by time-restricted feeding. Our phase-response curve analyses revealed that mice are most responsive to TRF entrainment at ZT0-4. Our data obtained from long-term, fiber photometry monitoring of intracellular Ca^{2+} signals in the SCN of freely moving mice provided evidence that the frequency of Ca^{2+} transients in SCN GABAergic neurons can be entrained by ZT0-4 TRF treatment. Our investigation revealed that the IGF2-KCC2 pathway in the SCN plays a functional role in sensing mealtime and therefore modulates the outcome presented including behavioral changes and sleep-awake cycle changes.

RESULTS

Time-restricted feeding entrainment generates persistent aftereffects in locomotor activity

To study the entrainment effect of time-restricted feeding (TRF) on locomotor activity independent of light/dark cues, we measured locomotor changes after TRF treatment under constant darkness. To do this, C57BL/6J mice (6–8 weeks of age) were housed individually in cages with a wheel under a 12:12 LD cycle for two weeks with free access to food (*ad libitum*). Then these mice were subjected to two weeks of TRF entrainment with 12 different 4-h TRF windows plus *ad libitum* feeding as a control (n = 6 per group, with a 2-h binning design). Afterward, all mice were released into constant darkness (DD) and returned to *ad libitum* feeding to measure the locomotor changes (Figure 1A, detailed information in STAR Methods). During the TRF period, food intake amount and body weight were measured. TRF mice showed reduced intake compared to *ad libitum*-fed mice (Figures 1 and S1A and Table S2 for two-way ANOVA). Accordingly, the body weights of the TRF mice recovered gradually after an initial reduction, but did not reach to the level of *ad libitum* fed mice at the end of TRF (Figures 1 and S1B and Table S2 for two-way ANOVA). During the TRF phase of the experiment, we observed premeal activity (i.e., virtually the same as the "anticipation activity") as described previously (Mistlberger et al., 2009; Pendergast and Yamazaki, 2018). However, such premeal activity disappeared soon after returning the animals to *ad libitum* fed and was released to DD (Figure 1B).

The most notable trend from this experiment was the effect of the TRF entrainment on delayed offset activity (i.e., the end time of activity) under DD. The impact of the ZT0-4 TRF (ZT0: lights on, ZT12: lights off) on mouse offset activity was much stronger than for any other windows (Figures 1B and 1C). Specifically, ZT0-4 TRF (indeed at the beginning of the light period phase) entrained mice displayed a significant delay of offset activity by determining an increased distance between the onset (i.e., the start time of activity) and offset activity in DD (Figure 1C). The splitting activity between onset and offset was as previously described (Kon et al., 2014). However, ZT0-4 TRF entrainment did not induce free-running period changes compared to *ad libitum* feeding using X^2 periodogram analysis (23.69 ± 0.06 versus 23.63 ± 0.23, $p > 0.05$). Furthermore, the extent of the free-running period assessed by their onset activity and offset activity was not significantly different in the ZT0-4 TRF-entrained mice (23.69 ± 0.06 vs. 23.68 ± 0.11, $p > 0.05$), suggesting that the activity rhythms remained constant.

To quantify the change in response to TRF entrainment, we also calculated the locomotion range by averaging the time between onset activity and offset activity for a total of 10 successive days after the mice were released to *ad libitum* feeding under DD. The phase-response curve (PRC) of TRF entrainment highlighted that the extent of the offset delay expanded from the ZT20-0 to ZT0-4 TRF windows and showed that an abrupt, unstable fluctuation followed the expansion at ZT2 (Figures 1C and 1D). These results indicated that ZT0-4 was the most TRF-sensitive time point (around the beginning of the light period phase). We detected only a weak impact on locomotor activity from the ZT8 to ZT18 TRF window, suggesting that these time windows might be "dead zones" for any TRF-mediated impacts.

Having detected that the ZT0-4 TRF window triggered the longest elongations of offset activity, we determined how many days these TRF-induced locomotor effects persisted. To test this duration, mice were exposed to a 2-week TRF entrainment (ZT0-4 TRF) and were then released into DD for an entire month with *ad libitum* fed in independent TRF cohorts. We found that TRF entrainment-induced locomotor plasticity lasted for at least one month (Figures 2A and 2B). Interestingly, when mice were directly released into a 12:12 LD cycle, the aftereffect induced by ZT0-4 TRF entrainment still persisted in independent TRF cohorts (Figures 2C and 2D), despite our expectation that this locomotor behavior change would be immediately suppressed by light. Furthermore, we applied saturating light pulses at circadian time CT0-1 (CT0 corresponds to subjective dawn, CT12 to subjective dusk) when the mice were released into constant darkness (DD), but observed no significant phase advances for onset or offset activity according to Clocklab analysis (Figures 2E and 2F), suggesting that ZT0-4 TRF-induced locomotor changes could not be masked by light.

Finally, we investigated whether shortening the TRF entrainment from two weeks to one week might affect locomotor plasticity. Under this condition, the mice still exhibited an extended locomotion range (Figures 2G and 2H). These results firmly establish that iterative restriction feeding in a time window around ZT0-4 induced robust and persistent changes in locomotor behavior and emphasized outsized impacts of this particular TRF window on mouse locomotor activity compared to TRF at other times of the day.

Neuronal activation in the SCN of freely moving mice corresponds to the observed locomotor plasticity

Having identified that TRF induced sustained locomotor plasticity, occurring every day and persisting under DD or 12:12 LD, we then searched for the neuronal basis for this behavioral phenotype. Given the known role of the suprachiasmatic nucleus (SCN) in both the regulation of the circadian clock and the output of locomotion behavior (Hastings et al., 2018; Herzog et al., 2017; Inagaki et al., 2007; Mei et al., 2018; Shan et al., 2020), we focused on this brain region. We established a recording system to monitor intracellular Ca^{2+} signals in the SCN of freely moving mice by using a jGCaMP7s, a high-performance (GFP-based) Ca^{2+} sensor (Dana et al., 2019), a custom high-numerical-aperture (0.5 NA) to increase signal-to-noise ratios and a custom-designed dual-color optical fiber for photometry, with a Ca^{2+}-dependent excitation wavelength at 470 nm and a Ca^{2+}-independent isosbestic excitation wavelength of 410 nm (Figures S2A–S2C).

To study the characteristics of SCN neuronal activity, we injected an adeno-associated virus encoding Cre-dependent jGCaMP7s (together with AAV encoding Cre with GABA transporter (VGAT) promoter) into the SCN (Figures S2A and S2B). We recorded Ca^{2+} signals originating from GABAergic neurons in the SCN of freely moving mice after three weeks for full viral expression (Figure S2D). The signal was then recorded for 35 s every 10 min to reduce the phototoxicity to the SCN neurons using a custom Iper Studio Alpha script. Another custom-developed script was used for data extraction as well as qualitative analysis of changes in different frequencies of Ca^{2+} signals (spectral analysis) for the long-term recording dataset. Changes in fluorescence over baseline fluorescence ($\Delta F/F$) were calculated as previously described (Jones et al., 2018).

We observed robust daily rhythms of intracellular Ca^{2+} transients in SCN GABAergic neurons. The mean Ca^{2+} signals for SCN GABAergic neurons were almost 3× higher during the subjective daytime than at subjective nighttime (Figure S2D). At lights on, Ca^{2+} signals exhibited gradually ascending signals (approximately CT22 to CT24), whereas at lights off, Ca^{2+} signals fell quickly (approximately CT35 to CT37). The transition between the rising and falling phases of the Ca^{2+} signals corresponded separately to the end of offset activity and the onset of activity around the lights on and light off (Figure S2D). The changes in Ca^{2+} signals reflected a real-time locomotor state, suggesting that Ca^{2+} signals enabled us to dissect functional changes corresponding to the onset or offset of locomotor activity.

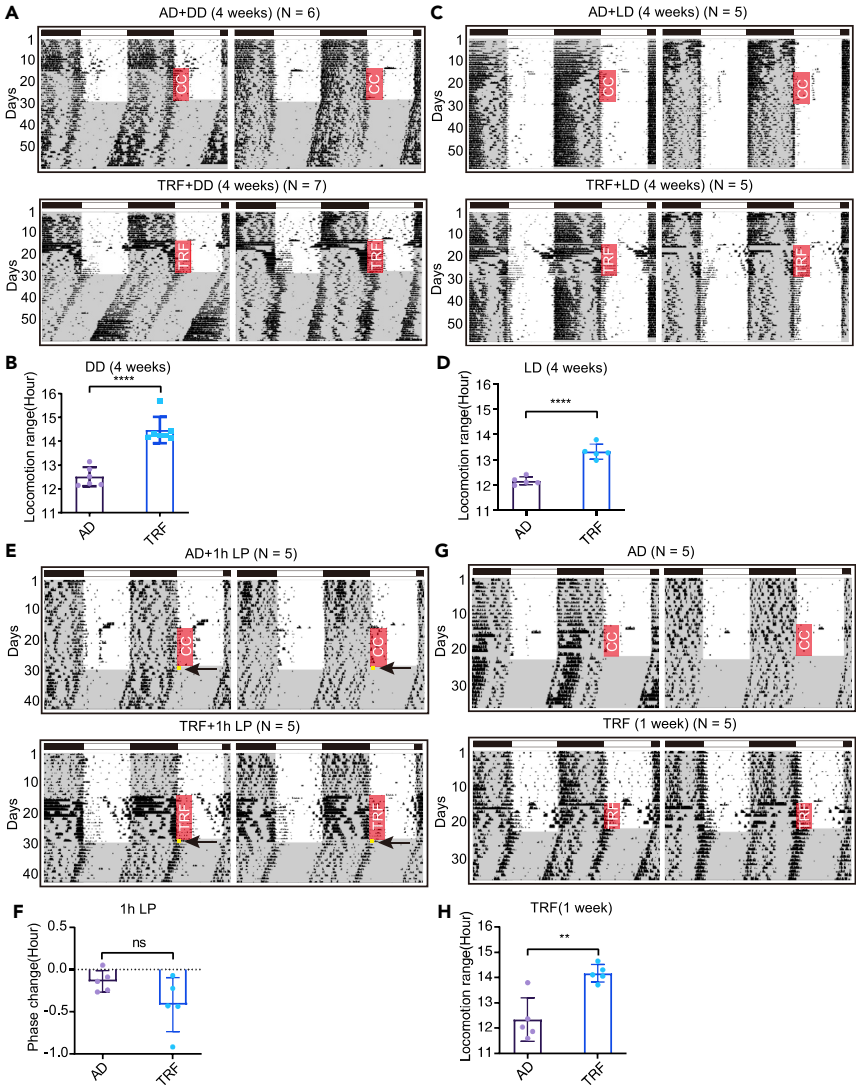

Figure 2. Robust aftereffect induced by ZT0-4 TRF

(A) Two representative actograms of mice administered 2 weeks of TRF (n = 7) and released to DD and *ad libitum* for 4 weeks with *ad libitum* as the control (n = 6). CC means that cages were changed with food and thereafter.

(B) Statistical analysis of locomotion range under DD in the TRF and *ad libitum* groups for a total of 28 successive days.

(C) Two representative actograms of mice administered 2 weeks of TRF (n = 5) and released to LD and *ad libitum* for 4 weeks with *ad libitum* as the control (n = 5).

(D) Statistics of locomotion range under DD in the TRF and *ad libitum* groups.

(E) Two representative actograms of mice administrated 2 weeks of TRF (n = 5) and released to DD and *ad libitum* for 2 weeks with *ad libitum* as the control (n = 5). On the first day of DD, a 200 lux light pulse (LP) was given at CT0-CT1 for 1 hour (yellow rectangle and black arrow).

(F) Statistical analysis of the phase shift under DD in the TRF and *ad libitum* groups.

(G) Two representative actograms of mice administered 1 week of TRF (n = 5) and released to DD and *ad libitum* for 2 weeks with *ad libitum* as the control (n = 5).

(H) Statistical analysis of locomotion range under DD in the TRF and *ad libitum* groups. Values represent the average ±SD, **: $p < 0.01$, ****: $p < 0.0001$, ns: not significant. All p values are from two-tailed Student's *t*-tests.

TRF induces alteration of SCN GABA neuronal activity and its outputs

To assess whether TRF-induced locomotor plasticity was related to patterns of SCN neuronal activity, we designed an experiment including: a) recording of Ca^{2+} signals for over 84-h *ad libitum* fed phase (i.e., before TRF), b) a ZT0-4 TRF (including ZT8-ZT12 TRF for comparative analysis) entrainment for 2 weeks without recording signals, and finally, c) recording of Ca^{2+} signals upon release of TRF-exposed mice

into DD for another 84-h *ad libitum* feeding phase (i.e., after TRF) (Figure 3A). We did not record signals during the TRF entrainment phase because the mice's excessive locomotor activity frequently broke the optical fibers. We used the same mice to compare the difference before and after TRF to avoid signal deviation caused by the difference in AAV expression and location of the optical fiber in different mice. We normalized the Ca^{2+} intensity of subjective ZT23-4 TRF window (pink solid rectangle, onset area) or subjective ZT7-12 TRF window (pink unfilled rectangle, offset area) by the corresponding day at ZT23-13 intensity (blue shadow) to eliminate signal difference caused by increased Ca^{2+} intensity because there was a two-week interval before and after TRF (Figures 3B–3J).

We observed a striking pattern in the frequencies of Ca^{2+} transients when we aligned the Ca^{2+} signals from the mice before and after ZT0-4 TRF: the Ca^{2+} transients for approximately 4 h during the subjective TRF window each day were much more intense in mice entrained with ZT0-4 TRF (Figure 3B, labeled by red stars). Specifically, the average Ca^{2+} transient frequency in such 4-h windows was 0.36 $\pm$ 0.04 (ranging from 1 to 7.5 Hz) in the ZT0-4 entrained mice and only 0.27 $\pm$ 0.04 (ranging from 1 to 7.5 Hz) for the same mice before the ZT0-4 entrainment (Figures 3B–3D, 3J, and S3). We detected no significant changes in Ca^{2+} transient frequency before and after the ZT8-12 TRF entrainment (Figures 3F–3H, 3J, and S4), confirming the extraordinary impact of ZT0-4 TRF. We confirmed the correct position of the fiber insertion in the SCN region and the expression of the GCaMP after each of the above experiments (Figures 3E and 3I). This ensured that the detected Ca^{2+} signals were indeed from the SCN. At a minimum, these observations indicate that TRF entrainment during ZT0-4 encodes highly rhythmic patterns of differential SCN GABAergic neuron activity that persist for days after TRF entrainment.

To further confirm whether the aftereffect induced by ZT0-4 TRF requires the SCN, we performed ZT0-4 TRF in the SCN lesioned mice. In the SCN sham control, ZT0-4 TRF entrainment induced an extended locomotion range (Figure S5), whereas SCN lesioned mice exhibited arrhythmic locomotion under LD cycles or ZT0-4 TRF entrainment under DD and did not display an aftereffect as observed in the SCN sham mice (Figure S5), supporting that the aftereffect induced by ZT0-4 TRF entrainment requires the SCN function.

SCN^{VIP} neurons represent integration points for photic and nonphotic sensory inputs (Acosta-Galvan et al., 2011). The activation of SCN^{VIP} neurons by bilateral injections of Cre-dependent hM3Dq into the SCN of heterozygous VIP-Cre mice at ZT4 and ZT13 does not change locomotor or sleep-wake cycle phenotypes (Todd et al., 2020). Hence, we investigated whether selective inhibition of SCN^{VIP} neurons may simulate the effect of ZT0-4 TRF entrainment (i.e., delay the offset of activity). Thus, we injected AAV-DIO-hM4D(Gi)-mCherry into the SCN of VIP-Cre mice and administered the chemogenetic ligand clozapine N-oxide (CNO; 3 mg/kg) at ZT0 for 13 consecutive days (Figures S6A and S6B). During the daytime, the inhibition of SCN^{VIP} neurons did not delay locomotor activity offset (Figure S6C), indicating that simple activation or inhibition of SCN^{VIP} neurons during the daytime cannot directly affect locomotor plasticity (Collins et al., 2020). Alternatively, SCN^{VIP} neurons may not be involved in mediating TRF-related behaviors.

Given that TRF entrained SCN GABAergic neuronal activity, we wondered whether ZT0-4 TRF would induce an aftereffect of sleep-wake cycles. We conducted EEG and EMG recordings before and after the ZT0-4 TRF entrainment. The duration of nonrapid eye movement (NREM) and REM episodes after ZT0-4 TRF entrainment were decreased substantially in the subjective TRF windows (CT0-4, CT24-28, and CT48-52) (Figures 4A and 4B) compared to before TRF. Similar to increased locomotor activity, the wakefulness after ZT0-4 TRF entrainment was increased in the subjective TRF window (Figures 4C and 4D). Altogether, these sleep phenomena further reinforced the conclusions from ZT0-4 TRF induced the aftereffects of activity.

ZT0-4 TRF affects the expression of the ion transporters in the SCN

Given that ZT0-4 TRF entrainment specifically induced altered SCN neuronal activity at the beginning of the light period phase, we hypothesized that time-specific input information about feeding might induce changes in signaling activity in the SCN, reprogramming the SCN neuronal activity. We performed RNA-seq-based profiling of ZT0-4 TRF entrained SCN samples at CT1, CT7, CT13, and CT19 (CT1 represents 1 h after the subjective onset of daytime under constant-dark conditions) from the second day after release to *ad libitum* in experienced ZT0-4 TRF mice. To identify differentially expressed candidate genes, we included two additional sets of control samples: ZT8-12 TRF-entrained SCN samples and *ad libitum* SCN samples at CT1, CT7, CT13, and CT19. The expression profiles of core clock genes (*Bmal1, Clock, Per1, Per2, Cry1, Cry2*) from the ZT0-4 TRF-entrained SCN samples did not differ significantly from those

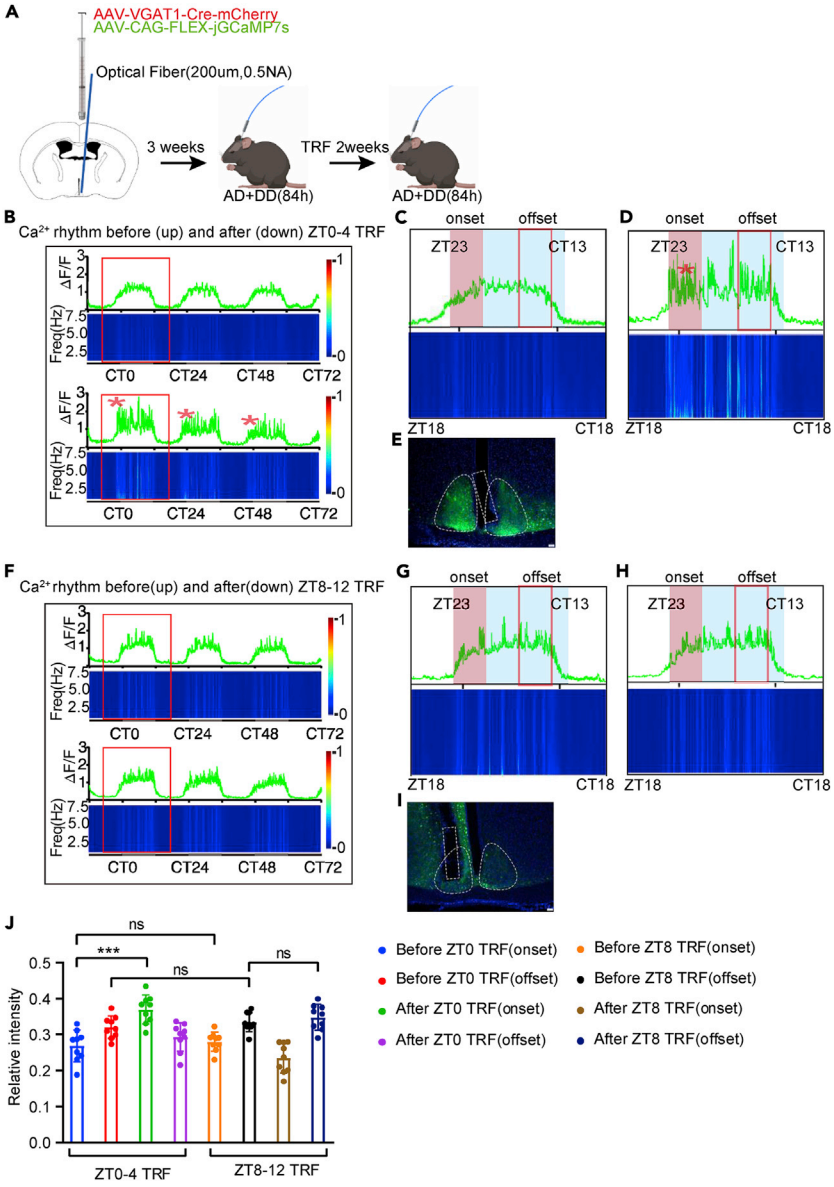

Figure 3. Elevated activities in the SCN GABAergic neuronal population by ZT0-4 TRF

(A) Experimental design of Ca^{2+} signal recording. The signal was collected before and after the TRF in the same mouse (n = 3 for 3 successive days).

(B) Ca^{2+} signals before (up) and after (down) TRF entrainment at ZT0-4. The heatmap shows the power of the Ca^{2+} signal at different wave frequencies which corresponds to the ΔF/F data. Red asterisks indicate a higher Ca^{2+} intensity region.

(C and D) A zoom in of the Ca^{2+} signal from the red unfilled rectangle in Figure B. Pink solid rectangle (onset area): the region intensity was calculated as the Ca^{2+} signal changes before and after TRF at ZT23-CT3 (See STAR Methods).

(E) The expression of GCamp7s (green) and DAPI (blue) and the location of optical fibers (white dotted box) in 50 μm SCN slice from ZT0-4 TRF mice. (Scale bar: 100 μm).

(F–H) The effect of the TRF entrainment at ZT8-ZT12 on Ca^{2+} signal recording as described in (B–D) (n = 3). Pink unfilled rectangle (offset area): The region intensity was calculated as the Ca^{2+} signal changes before and after TRF at CT7-CT11.

(I) The expression of GCamp7s (green) and DAPI (blue) and the location of optical fiber (white-dotted box) in 50 μm SCN slice from ZT8-12 TRF mice. (Scale bar: 100 μm).

(J) Relative intensity of the Ca^{2+} signal before or after TRF. The frequency power in 1 h before the subjective ZT0-4 TRF window (ZT23-CT3, CT23-CT27, CT47-CT51, onset area) and ZT8-12 TRF window (CT7-CT11, CT31-CT35, CT55-CT59, offset area) were normalized by the total Ca^{2+} signal in corresponding active phase (ZT23-CT13, CT23-CT37, CT47-CT61, blue area). Values represent the average ±SD, ***: $p < 0.001$, ns: not significant. All p values are from two-tailed Student's *t*-tests. See also Figures S2–S6.

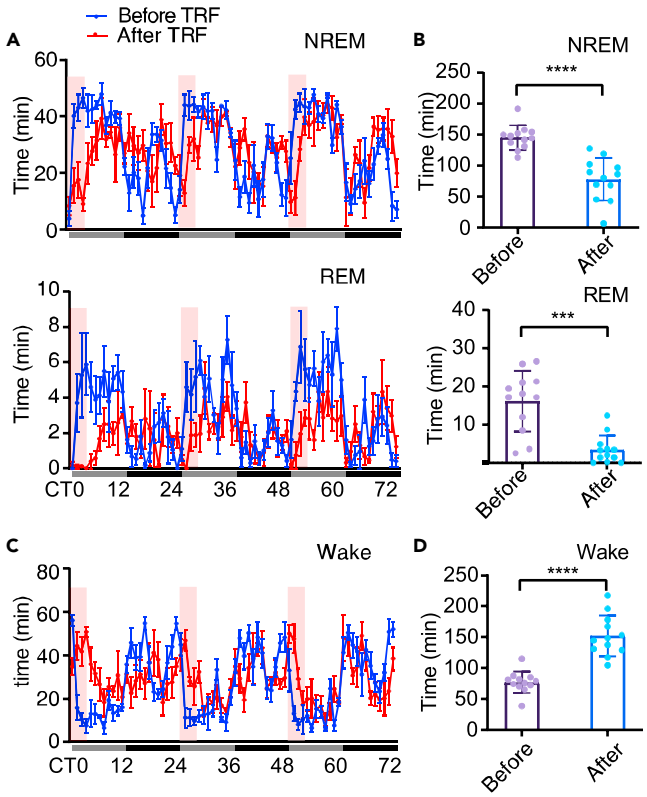

Figure 4. ZT0-4 TRF induces the aftereffect in the sleep-wake cycle

(A) Changes in NREM sleep and REM sleep before and after ZT0-4 TRF under constant darkness. Values represent the average ±SEM, (n = 4). Red rectangle: subjective TRF window.

(B) Total time spent in NREM and REM in the subjective TRF window (CT0-CT4, CT24-CT28, CT48-CT52) before or after TRF. Values represent the average ±SD, ***: $p < 0.001$, ****: $p < 0.0001$. All p values are from two-tailed Student's *t*-tests.

(C) Changes in wake-up time before and after ZT0-4 TRF under constant darkness. Values represent the average ±SEM, (n = 4). Red rectangle: subjective TRF window.

(D) Total time spent in wakefulness in the subjective TRF window (CT0-CT4, CT24-CT28, CT48-CT52) before or after TRF. Values represent the average ±SD, ****: $p < 0.0001$. The p value is from two-tailed Student's *t* test.

of the ZT8-12 and *ad libitum* groups (Figure 5A and S7). However, we did detect a dampened amplitude for the expression of *Nr1d1* at CT7 and *Dbp* at CT13 in the ZT0-4 TRF-entrained animals (Figure S7). To further confirm whether the molecular clock in the SCN was changed after ZT0-4 TRF, we collected ZT0-4-entrained SCN samples at 4-h intervals. The RT-PCR results showed that the expression patterns of the core clock genes *Bmal1*, *Per1*, and *Per2* and the clock-controlled genes *Avp* and *Pk2* showed slightly different patterns but did not reach statistical significance except for *Bmal1* ($p = 0.0497$) in the ZT0-4 TRF group (Figure S8).

Principal component analysis (PCA) performed on the raw RNA-seq data (n = 3 per time point) after Bartlett's test revealed that CT1 samples from ZT0-4 TRF (blue dots) were distinct from the control samples (*ad libitum*) and the other ZT0-4 TRF and ZT8-12 TRF samples with evident separation along PC1 (Figure 5B), suggesting that ZT0-4 TRF specifically reprogrammed the transcriptome of the SCN samples at CT1. Notably, this cluster of genes might correspond to the observed high frequency of Ca^{2+} transients and might represent SCN neuronal activity changes. To analyze which transcripts exerted the most significant influence on PC1 in this model, we used the cos^2 values to scale their relative importance (Nikhil et al., 2020). We shortlisted the top 214 genes that met $cos^2 > 0.5$, and found that 142 genes among 214 genes had significantly different expression in the ZT0-4 TRF entrained SCN in CT1 samples compared with other groups (see details in the STAR Methods). Significant KEGG enriched pathways included ECM-receptor interaction and focal adhesion (Figure 5C). Significant GO terms of the "Molecular function" included collagen-binding extracellular matrix binding and calcium binding. Significant GO terms of the "Cell

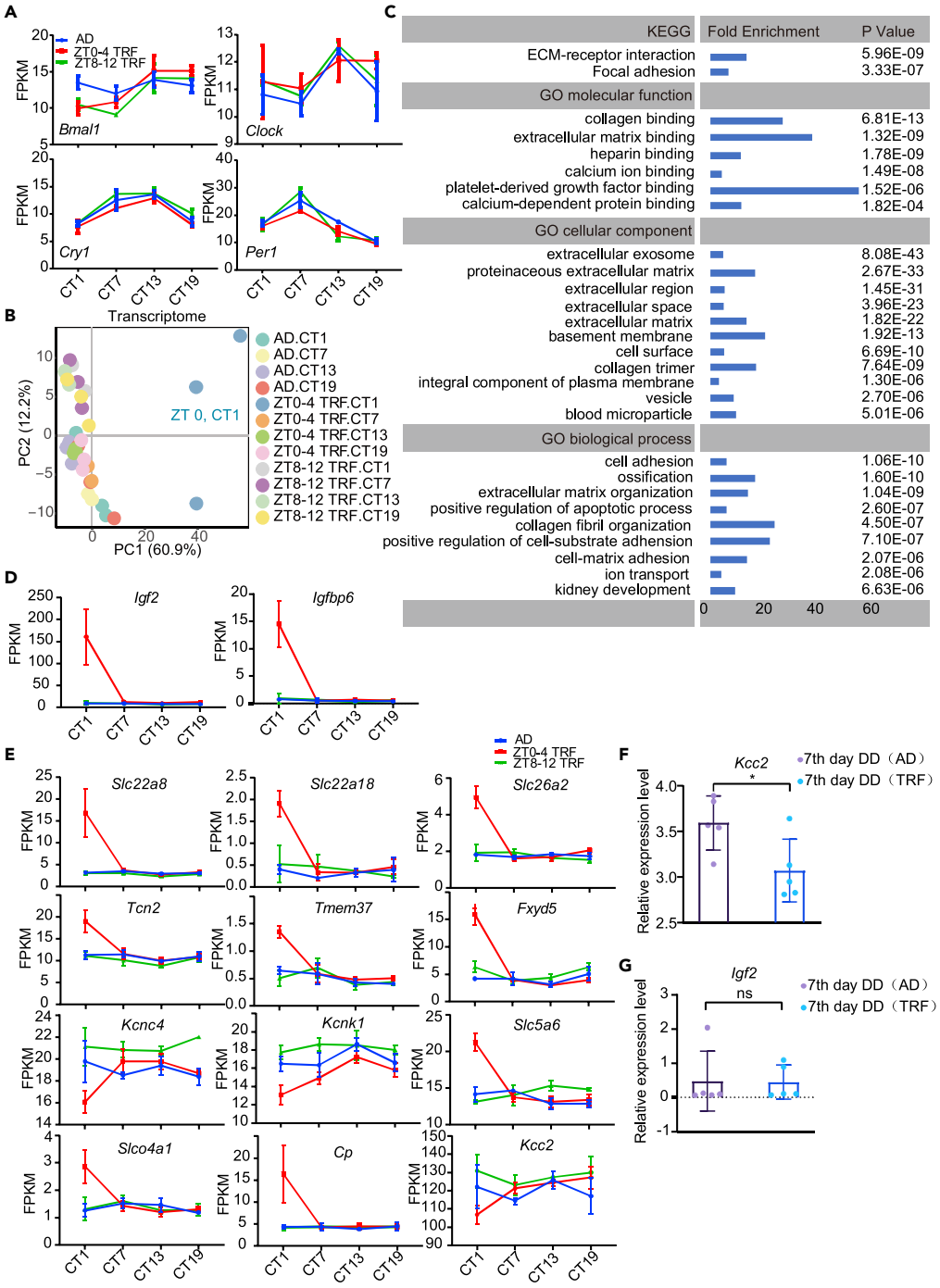

Figure 5. RNA profiling of the SCN samples showed the distinct transcriptome by the TRF entrainment at ZT0-4

(A) FPKM of clock genes in the *ad libitum*, ZT0-4 TRF, and ZT8-12 TRF entrainment groups. n = 3 per time point.

(B) PCA of SCN RNA-seq data at CT1, CT7, CT13 and CT19 in three groups: ZT0-4 TRF, ZT8-12 TRF and *ad libitum*, (n = 3 per time point).

(C) KEGG and GO pathway analysis of the 142 most relevant genes.

(D) Changes in *Igf2* and *Igfbp6* in the *ad libitum*, ZT0-4 TRF, and ZT8-12 TRF entrainment groups.

(E) Change in ion transport in the *ad libitum*, ZT0-4 TRF, and ZT8-12 TRF entrainment groups.

(F and G) Relative expression levels of *Kcc2* (F) and *Igf2* (G) in the CT0 SCN samples of the seventh day after ZT0-4 TRF under constant darkness in both the *ad libitum* control and ZT0-4 TRF groups. Values represent the average ±SD, *: $p < 0.05$, ns: not significant. All p values are from two-tailed Student's *t*-tests. See also Figures S7 and S8.

component" included extracellular exosome, and the "Biological process" included ion transport (Figure 5C). Most of the significantly differentially expressed genes (DE-Gs) were related to various collagen proteins, which were previously reported to maintain structural and functional neuroplasticity by modulating Ca^{2+} and K^{+} channels and modulating intracellular Ca^{2+} concentrations (Figure 5C) (Cho et al., 2018).

IGF2 belongs to the family of insulin-like peptides and has general roles in growth, metabolism, and aging (Beletskiy et al., 2021; Fernandez and Torres-Aleman, 2012). The expression of *Igf2* can be induced following learning training and this increase is essential for memory consolidation (Chen et al., 2011; Stern et al., 2014). Notably, the most significantly upregulated genes identified were insulin-like peptide Factor 2 (*Igf2*) and IGF-binding protein 6 (*Igfbp6*) (Figure 5D). We also found that ZT0-4 TRF entrainment caused reprogramming of genes for ion transport, including *Kcc2, Slc26a2, Slc13a3, Slc5a6, Slc22a18, Slc26a7, Slc22a8, Slc04a1, Kcnc4, Kcnk1, Tspo, Fxyd5, Wnk4, Cp, Cybb, Tmem37, Tcn2,* and *Clic1* (Figure 5E). Of these ion channel-related genes, *Kcc2* was the most enriched in the SCN and encoded a potassium-chloride cotransporter protein previously reported to entrain mice to long-day conditions (Olde Engberink et al., 2018; Rohr et al., 2019). To test whether there was a persistent change in the expression of *Kcc2* and *Igf2*, we examined the expression of *Kcc2* and *Igf2* using the SCN samples collected at the seventh day after release to *ad libitum* and DD in ZT0-4 TRF-entrained mice. We found that the level of *Kcc2* expression significantly decreased in TRF SCN compared with *ad libitum* SCN (Figure 5F), implying that the decrease in *Kcc2* may be related to the TRF-induced long-term locomotion change. Interestingly, the expression levels of *Igf2* recovered to normal levels after withdrawing TRF (Figure 5G), suggesting that the expression of *Igf2* may reflect an acute energy state in the SCN.

Ion channels are significant regulators of functional SCN pacemaker formation, including responses to photoperiod changes (Choi et al., 2008; Farajnia et al., 2014; Itri et al., 2005; Meredith et al., 2006; Myung et al., 2015). The similarities between the previously reported seasonal-change-induced phenotypes upon *Kcc2* disruption and our ZT0-4 TRF entrainment-induced downregulation of *Kcc2*, imply that KCC2 may also encode food entrainment information.

KCC2 encodes food intake-derived signals in the SCN that control locomotor outputs

To test the effect of KCC2 on SCN entrainment, we first knocked down the *Kcc2* in the SCN GABAergic neurons by stereotactically injecting AAV-VGAT-Cre and AAV-Ef1a-mCherry-U6-Loxp-CMV-EGFP-loxp-shRNA (*Kcc2*) or scramble shRNA into the SCN, enabling VGAT-Cre-dependent expression of the shRNA (Figures S9A and S9B). Locomotor activity was monitored, and the expression of KCC2 and AAV-derived mCherry in all mice was examined by immunostaining or fluorescence detection to ensure that *Kcc2* was specifically knocked down in SCN GABAergic neurons (Figure 6A).

Behavioral analysis revealed that knockdown of *Kcc2* in the GABAergic neurons of the SCN significantly increased the locomotion range even without TRF (Figures 6A and 6E). Because the circadian oscillation in the posterior SCN was phase-locked to the offset of activity, whereas the anterior SCN was phase-locked to the onset of activity (Inagaki et al., 2007), this decompression of the onset and offset of daily activity is most likely a consequence of reduced posterior SCN neuronal and anterior SCN neuronal coupling strength. *Kcc2* is known to mediate SCN coupling, and a previous study demonstrated that KCC2 encodes seasonal plasticity information (Myung et al., 2015; Rohr et al., 2019). Although ZT0-4 TRF widened the locomotor range in the scramble control, knocking down *Kcc2* further enhanced the widening of the locomotor phenotype under DD with larger onset and offset activity dispersions (Figures 6B and 6E). TRF at ZT8-12 cannot make the locomotor range wider in the scramble control, whereas knocking down *Kcc2* in SCN widens the locomotor range by ZT8-12 TRF (Figures 6C and 6E). We hypothesized that under normal/WT conditions, the SCN neuronal coupling is strong at ZT8-12, so it cannot widen the locomotor range; however, knocking down *Kcc2* decreases the coupling of SCN, and consequently, ZT8-12 TRF can make the changes.

Despite VGAT-Cre targeting more SCN cells, it has limitations, such as limited target locus selectivity and ectopic expression. To further confirm the effect of *Kcc2* knockdown in the SCN on locomotion regulation, we injected Cre-dependent shRNA (*Kcc2*) AAV into an SCN-specific Cre transgenic mice expressing the neuropeptide neuromedin S (NMS) (Figures S9C and S9D). The NMS neurons represent approximately 40% of all SCN neurons and decrease the impairment of RNAi interference in the SCN (Lee et al., 2015).

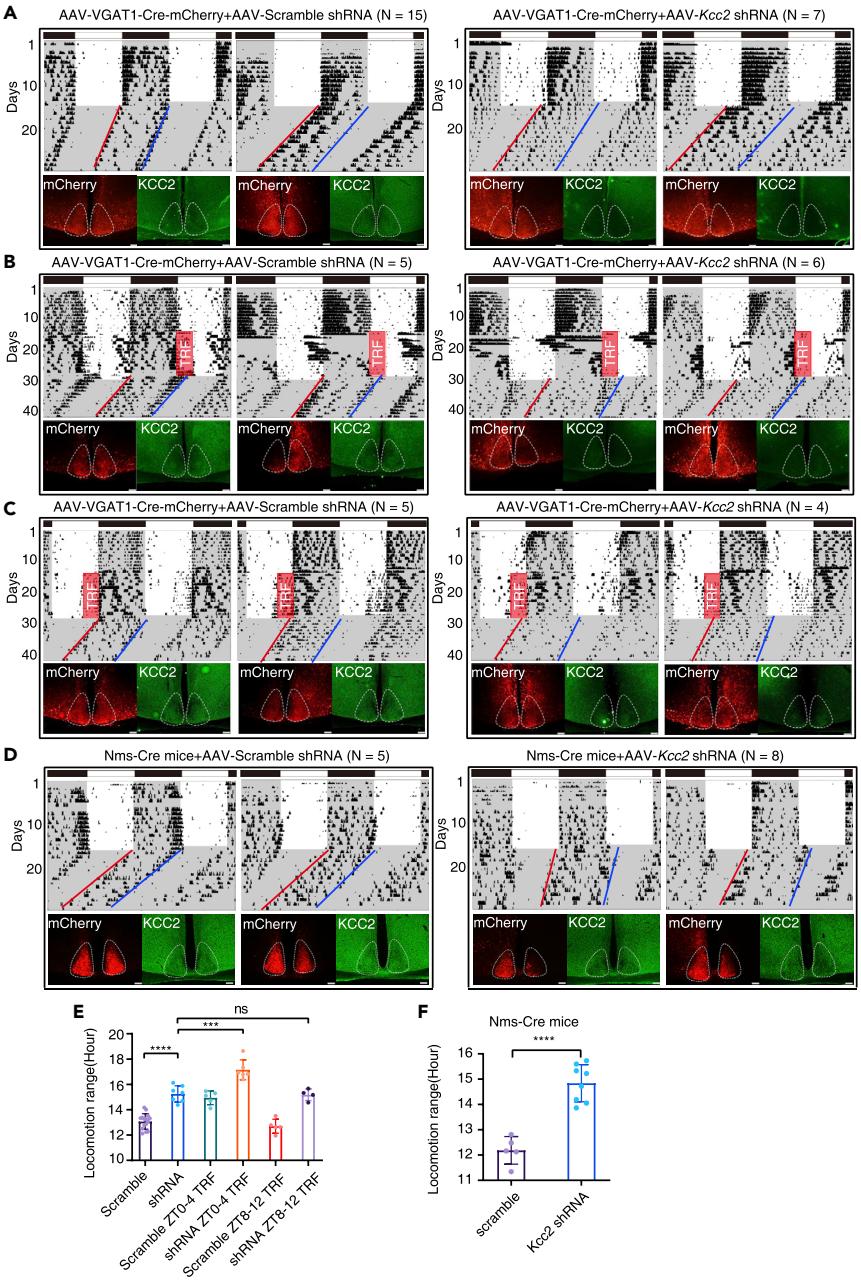

Figure 6. *Kcc2* knockdown in SCN GABAergic and NMS neurons increased the free-running locomotion range

(A) Two representative actograms of locomotors in control (n = 15) and *Kcc2* knockdown (n = 7) mice injected with AAV-VGAT-Cre and Cre inducible scramble or *Kcc2* shRNA in the SCN. All mice were entrained under LD for 2 weeks and then released to DD for 2 weeks. The expression of KCC2 (green) was verified by KCC2 antibody in SCN slices after experiments. The AAV injection site (red) was also verified by SCN slices. (Scale bar: 100 μm).

(B) Two representative actograms of locomotors in the control (n = 5) and *Kcc2* knockdown (n = 6) mice after 2 weeks of ZT0-4 TRF entrainment. (Scale bar: 100 μm).

(C) Two representative actograms of locomotors in the control (n = 5) and *Kcc2* knockdown (n = 4) mice after 2 weeks of ZT8-12 TRF entrainment. (Scale bar: 100 μm).

(D) Two representative actograms of locomotors in the control (n = 5) and *Kcc2* knockdown (n = 8) in NMS-Cre mice.

(E) Statistical analysis of the locomotion range of each group in (A), (B) and (C).

(F) Statistics of the locomotion range in NMS-Cre mice. Values represent the average ±SD, ****: $p < 0.0001$, ns: not significant. All p values are from two-tailed Student's *t*-tests. See also Figure S9.

Similarly, in Figure 6A we show that knocking down *Kcc2* using NMS-Cre can phenocopy the effect of TRF ZT0-4 on the locomotor range, whereas control mice had no extra effect (Figures 6D and 6F). Together with the VGAT-Cre data, these data suggest that TRF ZT0-4 widens the locomotor range through decreased SCN coupling mediated by *Kcc2*.

Altogether, our results show that depletion of *Kcc2* in SCN neurons exacerbates TRF-entrained locomotor plasticity, supporting the notion that the KCC2 could help the SCN adapt to feeding time and then behavioral output.

IGF2/KCC2 mediates ZT0-4 TRF induced locomotor changes

Considering that the effect of IGF2 as a memory and synaptic plasticity enhancer is robust, we speculated whether IGF2 is involved in sensing the energy state and therefore modulates SCN output. Unexpectedly, knockdown of *Igf2* in the SCN GABAergic neurons led to complete loss of daily locomotor rhythm (Figure S10). DAPI staining also showed a loss in the SCN neurons (Figure S10). These results reveal that IGF2 is an essential gene for proper SCN functioning.

Then, we used pharmacologic inhibitors to explore the function of IGF2 in TRF-induced locomotion regulation. A stainless brain cannula (RWD brain infusion kit) connected to the pump was inserted in the SCN, and IGF2 inhibitor-Chromeceptin or IGF1R inhibitor-GSK1904529A or vehicle (5% DMSO, 20% PEG300 and 75% saline) was administered for two weeks during ZT0-4 TRF. Notably, inhibition of IGF2 signaling completely abolished the aftereffect induced by ZT0-4 TRF (Figures 7A and 7B), suggesting that the observation of elevated *Igf2* in the ZT0-4 TRF-treated mice is responsible for delayed locomotor offset. Supporting no change in the expression of *Igf1*, the IGF1R inhibitor did not interfere with delayed locomotor offset, indicating that *Igf2* may represent a specific energy sensor in the SCN.

As ZT0-4 TRF significantly increases *Igf2* and *Igf2bp6* mRNA levels in the RNA-seq data, we then hypothesized that overexpressing IGF2 in the SCN could mirror the effect of TRF on the locomotor range. We thus overexpressed IGF2 in the GABAergic SCN neurons by injecting a mixture of AAV-VGAT-Cre and AAV-DIO-IGF2-EGFP or AAV-DIO-EGFP as described above (Figures S9E and S9F). Interestingly, the locomotion range increased significantly after overexpression of IGF2 in the GABAergic SCN neurons (Figures 7C and 7D). This phenotype observed in IGF2-overexpressing mice is largely mirrored by extended locomotion range induced by *Kcc2* knockdown (Figures 6A and 6D), suggesting a primary role of *Igf2* in the SCN in regulating the locomotor range.

The observed changes induced by IGF2 overexpression further reflect the correlation between *Igf2* and *Kcc2*. Along this line, we cultured rat SCN 2.2 cells, immortalized rat SCN cells (Allen et al., 2004), and treated SCN 2.2 cells with the recombinant IGF2 proteins at varying concentrations. The supplemented IGF2 demonstrated its ability to repress the expression of *Kcc2* in the presence of a high concentration of IGF2 (Figure 7E). This could explain why it induces locomotor range changes only in response to ZT0-4 TRF entrainment (i.e., high expression of *Igf2*).

Altogether, these results reveal that ZT0-4 TRF entrainment can induce the expression of *Igf2*, corresponding to decreased *Kcc2* levels that coordinate Ca^{2+} rhythm to behavior output, hinting toward food-seeking adaptation through nutritional demands(Figure 7F).

DISCUSSION

This study found that iterative ZT0-4 TRF entrainment results in an aftereffect on the delayed time of the end of locomotor activity and affects the sleep-wake cycle manifesting as a persistent behavioral change. We determined that the entrainment of the SCN by ZT0-4 TRF mediated locomotor changes occurs through regulating the IGF2/KCC2 pathway in SCN GABAergic neurons by *in vivo* intervention and recording Ca^{2+} signaling methods. The remarkable induction of *Igf2* and therefore decreased *Kcc2* expression by ZT0-4 TRF indicates that feeding time has a pleiotropic effect on the SCN functioning.

Previous studies found that the SCN can become sensitive to food availability in some species and under some conditions (Abe et al., 2007; Castillo et al., 2004; Escobar et al., 2020; Reinke and Asher, 2019), but its mechanism and function were not established. We provide fresh insight into entrainment of the SCN

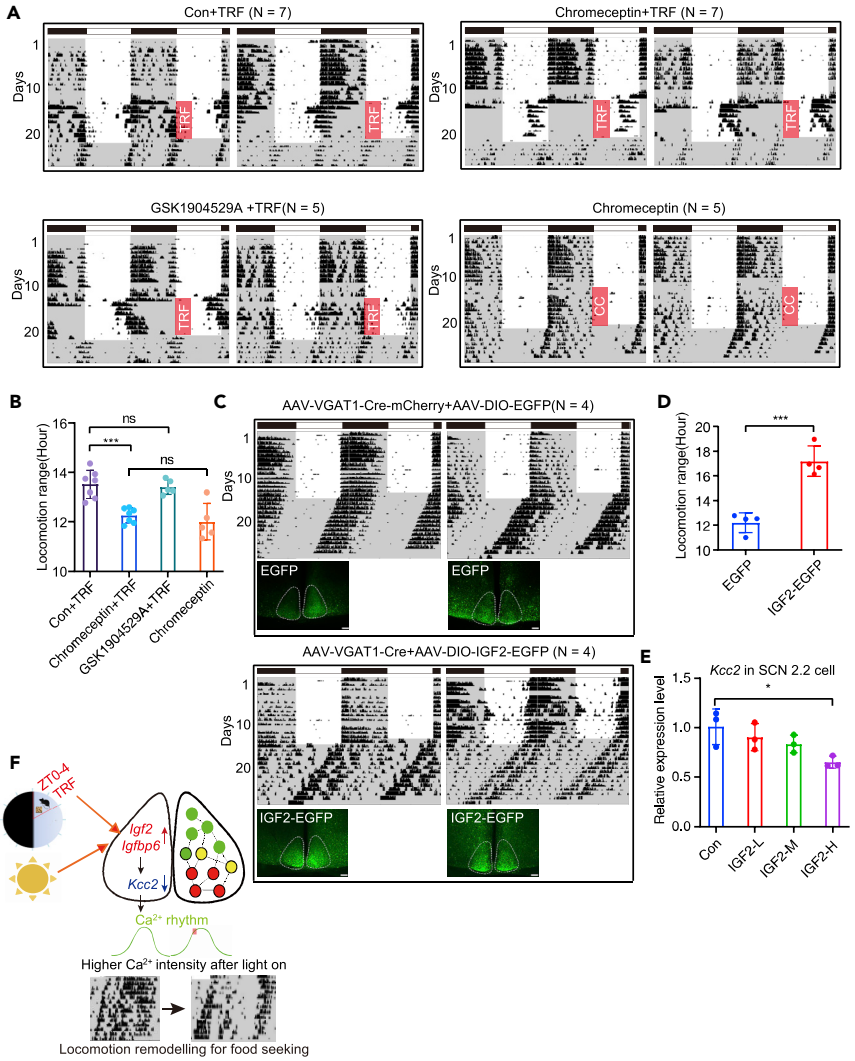

Figure 7. The IGF2-KCC2 pathway regulates the aftereffect of the ZT0-4 TRF on locomotion changes

(A) Two representative actograms of control (n = 7), IGF2 inhibitor-Chromeceptin (n = 7) and IGF1R inhibitor-GSK1904529A (n = 5) treated mice that were administered with 1 week of TRF entrainment and Chromeceptin (n = 5) treated mice with cage changes.

(B) Statistical analysis of locomotion range under DD in control, IGF2R inhibitor GSK1904529A, IGF2 inhibitor Chromeceptin-treated TRF-entrained mice and Chromeceptin-treated mice without TRF.

(C) A mixture of AAV-VGAT-Cre and AAV with Cre inducible EGFP and IGF2 was injected into the SCN of wild-type mice. Two representative actograms of locomotors in SCN GABAergic neurons EGFP-overexpressing control (n = 4) and IGF2-overexpressing mice (n = 4). All mice were entrained under LD for 2 weeks and then released to DD for 2 weeks. The AAV injection site (green) was also verified by SCN slices. (Scale bar: 100 μm).

(D) Statistics of the locomotion range for EGFP- and IGF2- overexpressing mice.

(E) The *Kcc2* mRNA expression in rat SCN 2.2 cells administered with PBS, a low concentration of IGF2 (IGF2-L, 5 ng/mL), a moderate concentration of IGF2 (IGF2-M, 50 ng/mL) and a high concentration of IGF2 (IGF2-H, 500 ng/mL).

(F) The working model of the effect of ZT0-4 TRF on SCN. ZT0-4 TRF affects the SCN plasticity by regulating *Igf2* signaling and thereby ion transport *Kcc2*, and finally influence the circadian output such as the neuron Ca^{2+} rhythm, sleep-wake cycle and locomotion range. Values represent the average ±SD , *: $p < 0.05$, ***: $p < 0.001$, ns: not significant. All p values are from two-tailed Student's *t*-tests. See also Figure S10.

by screening different feeding times with a 2-h interval. Our results clearly showed that the SCN can respond and adapt to changes in feeding availability, but this entrainment by feeding time is only limited at the beginning of the light period phase. ZT0-4 TRF did not affect the expression of core clock genes,

which is consistent with previous observations (Damiola et al., 2000; Stokkan et al., 2001). In our model, the ZT0-4 TRF induced the expression of *Igf2* coincided with the downregulation of *Kcc2* expression that accordingly changed the SCN neuronal activity and facilitated communication of feeding time with locomotor adaptation (Figure 7E). In a previous study, the feeding-associated hormones insulin and insulin-like growth Factor 1 (IGF1) was identified as global synchronized cue for mammalian circadian rhythms except for the SCN (Crosby et al., 2019). This is consistent with our result that pharmacological inhibition of the IGF1 receptor cannot abolish the aftereffect of ZT0-4 TRF entrainment, suggesting that the SCN neurons sense nutritional challenge and entrain to feeding cues different from peripheral tissues. Our studies indicate that IGF2 may be a key response gene that is consistent with its induced expression in the SCN accompanied by upregulation of IGF binding protein (IGFBP6), which has a 50 to 100-fold increased affinity for IGF2 over IGF1 (Bach, 2005) and further affect the expression of *Kcc2*.

Our data indicate that the persistent behavioral changes induced by ZT0-4 TRF entrainment are mirrored by changes in locomotor activity induced by seasonal photoperiod (Farajnia et al., 2014; Kon et al., 2014; Myung et al., 2015; Rohr et al., 2019). We show that the locomotor plasticity is associated with *Kcc2* downregulation in the SCN of TRF ZT0-4 entrained mice and resembles the decreased *Kcc2* levels observed in the SCN that receives and processes light input (Rohr et al., 2019). At a minimum, this resemblance suggests that downregulation of *Kcc2* is involved in SCN network recovery and is associated with locomotor behaviors after ZT0-4 TRF and after exposure to long-day conditions. Thus, a *Kcc2* related mechanism may likely represent an adaption for food-seeking behavior during seasonal changes. However, we acknowledge that TRF-induced reprogramming of ion transporters includes more than a dozen genes, and it is undoubtedly not only *Kcc2*.

The network of the SCN may represent a sensitive time window at the beginning of the light period phase that is susceptible to input signals. The rhythm in neural activity is built by the TTFL machinery, which has a precise phase relationship with entraining cues such as light. This epistatic relationship demonstrates that the SCN constitutes a fundamental translation element between the clock gene-mediated TTFL and rhythmic behavior (Colwell, 2011; Hastings et al., 2018; Herzog et al., 2017). In nocturnal animals, SCN neuron daytime activity is high and corresponds with behavioral quiescence in mice. However, we observed an unexpectedly higher intensity of Ca^{2+} signals during ZT0-4 derived from TRF entrained SCN, which parallels the increased locomotor activity. The potential function remains unclear, but several possibilities exist. One possibility is that the TTFL was not affected dramatically after TRF entrainment; thus, it is reasonable to view the daily changes in Ca^{2+} transients based on high amplitude expression rhythms linked to the TTFL mechanism. TRF stimulation may provide an ancillary interference to SCN-specific neurons, which may promote the activation of their target neurons for locomotor activity regulation. It is also possible that the higher Ca^{2+} frequency observed in TRF-entrained SCN may prevent light-induced phase shifts in the SCN and facilitate TRF-specific responses. We also cannot also rule out that the downregulation of *Kcc2* reverses the GABAergic neurons or NMS neurons from inhibitory to excitatory by increasing the intracellular Cl^{-}, which may change the characteristics of the region-SCN neurons to activate mouse locomotors. Although the underlying mechanisms warrant further investigation, this observation suggests that the SCN may contain different sensitive neurons to respond to environmental stimuli.

Indeed, it remains unclear why the beginning of the light period phase is the most sensitive time. One possibility, i.e., ZT0-4 TRF might cause a stronger select pressure than at any other time, where mice may prepare them to fall asleep and inhibit eating at the onset of light period phase, paralleling the scenario of only the 4-h food access. Under such a select pressure between maximal energy needs and maximal sleep pressure, mice may experience a demand-activated epigenetic program that induced *Igf2* expression rather than a circadian dependent cycle. At the electrophysiological level, likely, Ca^{2+} signal or electrophysiological rhythm at the onset of the light period phase responds to gradually ascending signals that are more easily disrupted by the expression of *Kcc2* than during quickly falling phase and other stable phases (the light period or the dark period phase). Again, TTFL was not affected dramatically after TRF entrainment; thus, we view the daily changes in Ca^{2+} transients based on high amplitude expression rhythms linked to the TTFL mechanism. Thus, future investigations on how the expression of *Igf2* is activated and impacts ion transports in the SCN could reveal how food intake timing affects the sleep wake cycles.

It bears strong emphasis that this higher frequency of Ca^{2+} transients in the ZT0-4 TRF-entrained mice persists, even for *ad libitum* fed mice, under DD and LD photo conditions. We interpret this to indicate that a learning component must be involved in this phenomenon, but any underlying mechanism(s) remain unknown. There is extensive evidence that memory formation is strongly affected by the time window of training and IGF2 can be activated during training (Chen et al., 2011; Stern et al., 2014), so identifying how this stable state is entrained in the SCN network should be a highly informative area of future work.

The present study shows that ZT0-4 TRF entrainment induces a robust aftereffect on the extended locomotor range and disruption of sleep/wake cycles. It is known from shift-workers and frequent airline travelers (jet-lag) that "internal desynchrony" can occur between internal rhythms and environmental cues (Bass and Takahashi, 2010), which can manifest as improper feeding time increased susceptibility to obesity, metabolic diseases, cardiovascular events, and cancer (Zarrinpar et al., 2016). Given our demonstration that this aftereffect originates from GABAergic neurons in the SCN, corresponding to the neuronal activity from inactivity to hyperactive transition which is the well-established similarity between nocturnal and diurnal mammals (Kuhlman, 2007), the ZT0-4 TRF (occurring at the onset of light period phase) may reflect a dawn circadian phenomena observed in humans. However, this translation requires caution because there is a large gap between diurnal and nocturnal animals.

Limitations of the study

A limitation is that it is hard to address whether *Igf2* is necessary for TRF genetically, because *Igf2* is an essential gene for SCN neuron survival, and knockdown of *Igf2* causes mouse arrhythmicity. A better animal model is needed to test whether knockdown SCN *Igf2* causes a loss of TRF aftereffects to fully validate the molecular mechanism of TRF on the SCN. As pointed out in the discussion, although these data suggest that IGF2 correlates with *Kcc2* expression, there is still a lack of mechanistic insights into how IGF2 or/and IGF2/KCC2 pathways communicate feeding time to locomotor behavior.

In addition, there are some technical limitations. It is hard to make every SCN neuron express the same amount of GCaMP or expected genes using AAV delivery technology that led to phenotype variations. Using SCN-specific Cre mice to mate with conditional knockin mice may enable more precise genetic manipulation of SCN in the future.

STAR★METHODS

Detailed methods are provided in the online version of this paper and include the following:

- KEY RESOURCES TABLE
- RESOURCE AVAILABILITY
  - Lead contact
  - Materials availability
  - Data and code availability
- EXPERIMENTAL MODEL AND SUBJECT DETAILS
  - Mouse strain
  - Cell lines and culture conditions
- METHODS DETAILS
  - Feeding schedule, food intake, and locomotor activity analyses
  - Stereotaxic viral injections
  - Ca^{2+} signal recording and signal analysis
  - SCN lesions
  - Sleep-wake monitoring and analysis
  - GSK1904529A, chromeceptin administration and osmotic pump implantation
  - SCN 2.2 culture and IGF2 administration
  - Immunofluorescence for SCN slice
  - RNA-seq and differently expressed genes analyses
  - PCA and Gene Ontology analysis
  - RT-PCR
- QUANTIFICATION AND STATISTICAL ANALYSIS

SUPPLEMENTAL INFORMATION

Supplemental information can be found online at https://doi.org/10.1016/j.isci.2022.104267.

ACKNOWLEDGMENTS

We thank members of Cam-Su GRC for their assistance in the animal facility and Xu's laboratory for discussion and Hongbo Jia for his critical reading. This work was supported by grants from the National Key R&D Program of China (2018YFA0801100) to Y.X., National Science Foundation of China (31630091) to Y.X., and the Science and Technology Project of Jiangsu Province (BZ2020067) to Y.X. We also thank the Priority Academic Program Development of the Jiangsu Higher Education Institutes (PAPD) and National Center for International Research (2017B01012). Vidal-Puig is supported by an MRC MDU grant.

AUTHOR CONTRIBUTIONS

Q.Z. and Y.X. conceived and designed the experiments. Q.Z. conducted time-restricted feeding, all behavioral analysis, AAV stereotactic injection, fiber photometry recordings, Ca^{2+} signal data analysis, sleep recording and analysis, chemogenetic manipulation, SCN *Kcc2* knockdown and IGF2 intervention experiments. Q.Z., Y.G., and Y.X. worked RNA-seq data analysis. Y.Z. assisted with the *Kcc2* knockdown experiment. Z.L. and B.Y. assisted with tissue sampling. J.Y. and L.Y. provided helps in Ca^{2+} signal data analysis. H.Q. and X.C. provided great helped with setting up the fiber photometry system. Q.Z., A.V-P., and Y.X. wrote the manuscript.

DECLARATION OF INTERESTS

The authors declare no competing interests.

Received: May 23, 2021
Revised: October 13, 2021
Accepted: April 13, 2022
Published: May 20, 2022

REFERENCES

Abe, H., Honma, S., and Honma, K.I. (2007). Daily restricted feeding resets the circadian clock in the suprachiasmatic nucleus of CS mice. Am. J. Physiol. Regul. Integr. Comp. Physiol. *292*, R607–R615. https://doi.org/10.1152/ajpregu.00331.2006.

Acosta-Galvan, G., Yi, C.X., van der Vliet, J., Jhamandas, J.H., Panula, P., Angeles-Castellanos, M., Del Carmen Basualdo, M., Escobar, C., and Buijs, R.M. (2011). Interaction between hypothalamic dorsomedial nucleus and the suprachiasmatic nucleus determines intensity of food anticipatory behavior. Proc. Natl. Acad. Sci. U S A. *108*, 5813–5818. https://doi.org/10.1073/pnas.1015551108.

Allen, G.C., Farnell, Y., Bell-Pedersen, D., Cassone, V.M., and Earnest, D.J. (2004). Effects of altered Clock gene expression on the pacemaker properties of SCN2.2 cells and oscillatory properties of NIH/3T3 cells. Neuroscience *127*, 989–999. https://doi.org/10.1016/j.neuroscience.2004.06.003.

Andrade, J.P., Pereira, P.A., Silva, S.M., Sa, S.I., and Lukoyanov, N.V. (2004). Timed hypocaloric food restriction alters the synthesis and expression of vasopressin and vasoactive intestinal peptide in the suprachiasmatic nucleus. Brain Res. *1022*, 226–233. https://doi.org/10.1016/j.brainres.2004.07.013.

Bach, L.A. (2005). IGFBP-6 five years on; not so 'forgotten'. Growth Horm. IGF Res. *15*, 185–192. https://doi.org/10.1016/j.ghir.2005.04.001.

Bass, J., and Takahashi, J.S. (2010). Circadian integration of metabolism and energetics. Science *330*, 1349–1354. https://doi.org/10.1126/science.1195027.

Beletskiy, A., Chesnokova, E., and Bal, N. (2021). Insulin-like growth factor 2 as a possible neuroprotective agent and memory enhancer-its comparative expression, processing and signaling in mammalian CNS. Int. J. Mol. Sci. *22*, 1849. https://doi.org/10.3390/ijms22041849.

Castillo, M.R., Hochstetler, K.J., Tavernier, R.J., Jr., Greene, D.M., and Bult-Ito, A. (2004). Entrainment of the master circadian clock by scheduled feeding. Am. J. Physiol. Regul. Integr. Comp. Physiol. *287*, R551–R555. https://doi.org/10.1152/ajpregu.00247.2004.

Challet, E. (2019). The circadian regulation of food intake. Nat. Rev. Endocrinol. *15*, 393–405. https://doi.org/10.1038/s41574-019-0210-x.

Chen, D.Y., Stern, S.A., Garcia-Osta, A., Saunier-Rebori, B., Pollonini, G., Bambah-Mukku, D., Blitzer, R.D., and Alberini, C.M. (2011). A critical role for IGF-II in memory consolidation and enhancement. Nature *469*, 491–497. https://doi.org/10.1038/nature09667.

Cho, S., Muthukumar, A.K., Stork, T., Coutinho-Budd, J.C., and Freeman, M.R. (2018). Focal adhesion molecules regulate astrocyte morphology and glutamate transporters to suppress seizure-like behavior. Proc. Natl. Acad. Sci. U S A. *115*, 11316–11321. https://doi.org/10.1073/pnas.1800830115.

Choi, H.J., Lee, C.J., Schroeder, A., Kim, Y.S., Jung, S.H., Kim, J.S., Kim, D.Y., Son, E.J., Han, H.C., Hong, S.K., and Colwell, C.S. (2008). Excitatory actions of GABA in the suprachiasmatic nucleus. J. Neurosci. *28*, 5450–5459. https://doi.org/10.1523/jneurosci.5750-07.2008.

Collins, B., Pierre-Ferrer, S., Muheim, C., Lukacsovich, D., Cai, Y., Spinnler, A., Herrera, C.G., Wen, S., Winterer, J., Belle, M.D.C., et al. (2020). Circadian VIPergic neurons of the suprachiasmatic nuclei sculpt the sleep-wake cycle. Neuron *108*, 486–499.e5. https://doi.org/10.1016/j.neuron.2020.08.001.

Colwell, C.S. (2011). Linking neural activity and molecular oscillations in the SCN. Nat. Rev. Neurosci. *12*, 553–569. https://doi.org/10.1038/nrn3086.

Crosby, P., Hamnett, R., Putker, M., Hoyle, N.P., Reed, M., Karam, C.J., Maywood, E.S., Stangherlin, A., Chesham, J.E., Hayter, E.A., et al. (2019). Insulin/IGF-1 drives PERIOD synthesis to entrain circadian rhythms with feeding time. Cell

177, 896–909.e20. https://doi.org/10.1016/j.cell.2019.02.017.

Damiola, F., Le Minh, N., Preitner, N., Kornmann, B., Fleury-Olela, F., and Schibler, U. (2000). Restricted feeding uncouples circadian oscillators in peripheral tissues from the central pacemaker in the suprachiasmatic nucleus. Genes Dev. *14*, 2950–2961. https://doi.org/10.1101/gad.183500.

Dana, H., Sun, Y., Mohar, B., Hulse, B.K., Kerlin, A.M., Hasseman, J.P., Tsegaye, G., Tsang, A., Wong, A., Patel, R., et al. (2019). High-performance calcium sensors for imaging activity in neuronal populations and microcompartments. Nat. Methods *16*, 649–657. https://doi.org/10.1038/s41592-019-0435-6.

Escobar, C., Espitia-Bautista, E., Guzman-Ruiz, M.A., Guerrero-Vargas, N.N., Hernandez-Navarrete, M.A., Angeles-Castellanos, M., Morales-Perez, B., and Buijs, R.M. (2020). Chocolate for breakfast prevents circadian desynchrony in experimental models of jet-lag and shift-work. Sci. Rep. *10*, 6243. https://doi.org/10.1038/s41598-020-63227-w.

Farajnia, S., van Westering, T.L., Meijer, J.H., and Michel, S. (2014). Seasonal induction of GABAergic excitation in the central mammalian clock. Proc. Natl. Acad. Sci. U S A. *111*, 9627–9632. https://doi.org/10.1073/pnas.1319820111.

Fernandez, A.M., and Torres-Aleman, I. (2012). The many faces of insulin-like peptide signalling in the brain. Nat. Rev. Neurosci. *13*, 225–239. https://doi.org/10.1038/nrn3209.

Fonken, L.K., and Nelson, R.J. (2014). The effects of light at night on circadian clocks and metabolism. Endocr. Rev. *35*, 648–670. https://doi.org/10.1210/er.2013-1051.

Hastings, M.H., Maywood, E.S., and Brancaccio, M. (2018). Generation of circadian rhythms in the suprachiasmatic nucleus. Nat. Rev. Neurosci. *19*, 453–469. https://doi.org/10.1038/s41583-018-0026-z.

Hastings, M.H., Maywood, E.S., and Brancaccio, M. (2019). The mammalian circadian timing system and the suprachiasmatic nucleus as its pacemaker. Biology *8*, 13. https://doi.org/10.3390/biology8010013.

Herzog, E.D., Hermanstyne, T., Smyllie, N.J., and Hastings, M.H. (2017). Regulating the suprachiasmatic nucleus (SCN) circadian clockwork: interplay between cell-autonomous and circuit-level mechanisms. Cold Spring Harb Perspect. Biol. *9*, a027706. https://doi.org/10.1101/cshperspect.a027706.

Houben, T., Deboer, T., van Oosterhout, F., and Meijer, J.H. (2009). Correlation with behavioral activity and rest implies circadian regulation by SCN neuronal activity levels. J. Biol. Rhythms *24*, 477–487. https://doi.org/10.1177/0748730409349895.

Inagaki, N., Honma, S., Ono, D., Tanahashi, Y., and Honma, K.I. (2007). Separate oscillating cell groups in mouse suprachiasmatic nucleus couple photoperiodically to the onset and end of daily activity. Proc. Natl. Acad. Sci. U S A. *104*, 7664–7669. https://doi.org/10.1073/pnas.0607713104.

Itri, J.N., Michel, S., Vansteensel, M.J., Meijer, J.H., and Colwell, C.S. (2005). Fast delayed rectifier potassium current is required for circadian neural activity. Nat. Neurosci. *8*, 650–656. https://doi.org/10.1038/nn1448.

Jones, J.R., Simon, T., Lones, L., and Herzog, E.D. (2018). SCN VIP neurons are essential for normal light-mediated resetting of the circadian system. J. Neurosci. *38*, 7986–7995. https://doi.org/10.1523/jneurosci.1322-18.2018.

Kelly, K.P., McGuinness, O.P., Buchowski, M., Hughey, J.J., Chen, H., Powers, J., Page, T., and Johnson, C.H. (2020). Eating breakfast and avoiding late-evening snacking sustains lipid oxidation. PLoS Biol. *18*, e3000622. https://doi.org/10.1371/journal.pbio.3000622.

Kon, N., Yoshikawa, T., Honma, S., Yamagata, Y., Yoshitane, H., Shimizu, K., Sugiyama, Y., Hara, C., Kameshita, I., Honma, K.I., and Fukada, Y. (2014). CaMKII is essential for the cellular clock and coupling between morning and evening behavioral rhythms. Genes Dev. *28*, 1101–1110. https://doi.org/10.1101/gad.237511.114.

Kuhlman, S.J. (2007). Biological Rhythms Workshop IB: neurophysiology of SCN pacemaker function. Cold Spring Harb Symp. Quant. Biol. *72*, 21–33. https://doi.org/10.1101/sqb.2007.72.061.

Lee, I.T., Chang, A.S., Manandhar, M., Shan, Y., Fan, J., Izumo, M., Ikeda, Y., Motoike, T., Dixon, S., Seinfeld, J.E., et al. (2015). Neuromedin s-producing neurons act as essential pacemakers in the suprachiasmatic nucleus to couple clock neurons and dictate circadian rhythms. Neuron *85*, 1086–1102. https://doi.org/10.1016/j.neuron.2015.02.006.

Liu, Z., Huang, M., Wu, X., Shi, G., Xing, L., Dong, Z., Qu, Z., Yan, J., Yang, L., Panda, S., and Xu, Y. (2014). PER1 phosphorylation specifies feeding rhythm in mice. Cell Rep. *7*, 1509–1520. https://doi.org/10.1016/j.celrep.2014.04.032.

Mei, L., Fan, Y., Lv, X., Welsh, D.K., Zhan, C., and Zhang, E.E. (2018). Long-term in vivo recording of circadian rhythms in brains of freely moving mice. Proc. Natl. Acad. Sci. U S A. *115*, 4276–4281. https://doi.org/10.1073/pnas.1717735115.

Meredith, A.L., Wiler, S.W., Miller, B.H., Takahashi, J.S., Fodor, A.A., Ruby, N.F., and Aldrich, R.W. (2006). BK calcium-activated potassium channels regulate circadian behavioral rhythms and pacemaker output. Nat. Neurosci. *9*, 1041–1049. https://doi.org/10.1038/nn1740.

Mistlberger, R.E. (2011). Neurobiology of food anticipatory circadian rhythms. Physiol. Behav. *104*, 535–545. https://doi.org/10.1016/j.physbeh.2011.04.015.

Mistlberger, R.E., Buijs, R.M., Challet, E., Escobar, C., Landry, G.J., Kalsbeek, A., Pevet, P., and Shibata, S. (2009). Food anticipation in Bmal1-/- and AAV-Bmal1 rescued mice: a reply to Fuller et al. J. Circadian Rhythms *7*, 11. https://doi.org/10.1186/1740-3391-7-11.

Myung, J., Hong, S., DeWoskin, D., De Schutter, E., Forger, D.B., and Takumi, T. (2015). GABA-mediated repulsive coupling between circadian clock neurons in the SCN encodes seasonal time. Proc. Natl. Acad. Sci. U S A. *112*, E3920–E3929. https://doi.org/10.1073/pnas.1421200112.

Nikhil, K.L., Korge, S., and Kramer, A. (2020). Heritable gene expression variability and stochasticity govern clonal heterogeneity in circadian period. PLoS Biol. *18*, e3000792. https://doi.org/10.1371/journal.pbio.3000792.

O'Neill, J.S., Maywood, E.S., Chesham, J.E., Takahashi, J.S., and Hastings, M.H. (2008). cAMP-dependent signaling as a core component of the mammalian circadian pacemaker. Science *320*, 949–953. https://doi.org/10.1126/science.1152506.

Olde Engberink, A.H.O., Huisman, J., Michel, S., and Meijer, J.H. (2020). Brief light exposure at dawn and dusk can encode day-length in the neuronal network of the mammalian circadian pacemaker. FASEB J. *34*, 13685–13695. https://doi.org/10.1096/fj.202001133rr.

Olde Engberink, A.H.O., Meijer, J.H., and Michel, S. (2018). Chloride cotransporter KCC2 is essential for GABAergic inhibition in the SCN. Neuropharmacology *138*, 80–86. https://doi.org/10.1016/j.neuropharm.2018.05.023.

Pendergast, J.S., and Yamazaki, S. (2018). The mysterious food-entrainable oscillator: insights from mutant and engineered mouse models. J. Biol. Rhythms *33*, 458–474. https://doi.org/10.1177/0748730418789043.

Reinke, H., and Asher, G. (2019). Crosstalk between metabolism and circadian clocks. Nat. Rev. Mol. Cell Biol. *20*, 227–241. https://doi.org/10.1038/s41580-018-0096-9.

Rohr, K.E., Pancholi, H., Haider, S., Karow, C., Modert, D., Raddatz, N.J., and Evans, J. (2019). Seasonal plasticity in GABAA signaling is necessary for restoring phase synchrony in the master circadian clock network. Elife *8*, e49578. https://doi.org/10.7554/elife.49578.

Schaap, J., Albus, H., VanderLeest, H.T., Eilers, P.H.C., Detari, L., and Meijer, J.H. (2003). Heterogeneity of rhythmic suprachiasmatic nucleus neurons: implications for circadian waveform and photoperiodic encoding. Proc. Natl. Acad. Sci. U S A. *100*, 15994–15999. https://doi.org/10.1073/pnas.2436298100.

Shan, Y., Abel, J.H., Li, Y., Izumo, M., Cox, K.H., Jeong, B., Yoo, S.H., Olson, D.P., Doyle, F.J., 3rd, and Takahashi, J.S. (2020). Dual-color single-cell imaging of the suprachiasmatic nucleus reveals a circadian role in network synchrony. Neuron *108*, 164–179.e7. https://doi.org/10.1016/j.neuron.2020.07.012.

Stern, S.A., Chen, D.Y., and Alberini, C.M. (2014). The effect of insulin and insulin-like growth factors on hippocampus- and amygdala-dependent long-term memory formation. Learn. Mem. *21*, 556–563. https://doi.org/10.1101/lm.029348.112.

Stokkan, K.A., Yamazaki, S., Tei, H., Sakaki, Y., and Menaker, M. (2001). Entrainment of the circadian clock in the liver by feeding. Science *291*, 490–493. https://doi.org/10.1126/science.291.5503.490.

Todd, W.D., Venner, A., Anaclet, C., Broadhurst, R.Y., De Luca, R., Bandaru, S.S., Issokson, L., Hablitz, L.M., Cravetchi, O., Arrigoni, E., et al. (2020). Suprachiasmatic VIP neurons are required for normal circadian rhythmicity and comprised of molecularly distinct subpopulations. Nat. Commun. *11*, 4410. https://doi.org/10.1038/s41467-020-17197-2.

VanderLeest, H.T., Houben, T., Michel, S., Deboer, T., Albus, H., Vansteensel, M.J., Block, G.D., and Meijer, J.H. (2007). Seasonal encoding by the circadian pacemaker of the SCN. Curr. Biol. *17*, 468–473. https://doi.org/10.1016/j.cub.2007.01.048.

Wang, T.A., Yu, Y.V., Govindaiah, G., Ye, X., Artinian, L., Coleman, T.P., Sweedler, J.V., Cox, C.L., and Gillette, M.U. (2012). Circadian rhythm of redox state regulates excitability in suprachiasmatic nucleus neurons. Science *337*, 839–842. https://doi.org/10.1126/science.1222826.

Welsh, D.K., Takahashi, J.S., and Kay, S.A. (2010). Suprachiasmatic nucleus: cell autonomy and network properties. Annu. Rev. Physiol. *72*, 551–577. https://doi.org/10.1146/annurev-physiol-021909-135919.

Zarrinpar, A., Chaix, A., and Panda, S. (2016). Daily eating patterns and their impact on health and disease. Trends Endocrinol. Metab. *27*, 69–83. https://doi.org/10.1016/j.tem.2015.11.007.

Zhang, Z., Zhai, Q., Gu, Y., Zhang, T., Huang, Z., Liu, Z., Liu, Y., and Xu, Y. (2020). Impaired function of the suprachiasmatic nucleus rescues the loss of body temperature homeostasis caused by time-restricted feeding. Sci. Bull. *65*, 1268–1280. https://doi.org/10.1016/j.scib.2020.03.025.

STAR★METHODS

KEY RESOURCES TABLE

REAGENT or RESOURCE	SOURCE	IDENTIFIER
Antibodies		
Rabbit polyclonal anti-KCC2	Proteintech	Cat#19565-1-AP;RRID:AB_10638485
Alexa Fluor 488 Donkey anti-rabbit IgG	ThermoFisher	Cat#A-21206;RRID:AB_2535792
Alexa Fluor 594 Goat anti-rabbit IgG	ThermoFisher	Cat#A-11037;RRID:AB_2534095
Bacterial and virus strains		
rAAV-VGAT1-Cre-mCherry-WPRE-pA	BrainVTA	Cat#PT-0533
rAAV-CAG-FLEX-jGCaMP7s-WPRE-SV40 pA	BrainVTA	Cat#PT-1421
rAAV-Ef1a-mCherry-U6-Loxp-CMV-EGFP-loxp-shRNA *(Kcc2)*	BrainVTA	Cat#PT-2146
rAAV-Ef1a-mCherry-U6-Loxp-CMV-EGFP-loxp-shRNA (Scramble)	BrainVTA	Cat#PT-0900
rAAV- Ef1α-DIO-mCherry-WPRE-pA	BrainVTA	Cat#PT-0013
rAAV-Ef1α-DIO-hM4D(Gl)-mCherry-WPREs	BrainVTA	Cat#PT-0043
rAAV-VGAT1-Cre-WPRE-pA	BrainVTA	Cat#PT-0346
rAAV- CMV-DIO -IGF2-2A-EGFP-WPRE-pA	BrainVTA	Cat#PT-2640
rAAV-Ef1a-mCherry-U6-Loxp-CMV-EGFP-loxp-shRNA (*Igf2*)	BrainVTA	Cat#PT-3409
rAAV-CMV-DIO-EGFP-WPRE-pA	BrainVTA	Cat#PT-0310
Chemicals, peptides, and recombinant proteins		
Recombinant Human IGF-2	Beyotime	Cat#P5538
GSK1904529A	MCE	Cat#HY-10524
Chromeceptin	Sigma	Cat#C0868
clozapine N-oxide	APExBIO	Cat#A3317
DMEM/HIGH GLUCOSE	HyClone	Cat#AF29483100
Fetal bovine serum	Gibco	Cat#10270
Pen/strep	Gibco	Cat#15070-063
DMSO	Sigma	Cat#D8418
PEG300	MCE	Cat#HY-Y0873
Trizol	ThermoFisher	Cat#GB15596-018
Isoflurane	RWD	Cat#845AS-1010015
DAPI	Sigma	Cat#D9542
GlycoBlue	ThermoFisher	Cat#AM9515
Deposited data		
Raw RNAseq data	This paper	[SRA]:[PRJNA705298]
Experimental models: Cell lines		
Rat:SCN 2.2	Kerafast (from the laboratory of David J. Earnest)	Cat#EUT500
Experimental models: Organisms/strains		
Mouse: C57BL/6J	GemPharmatech; Charles River Laboratories	Cat#N000013; Cat#219
Mouse: B_6/JGpt-Vip$^{em1Cin(iCre)}$/Gpt	Soochow University	N/A
Mouse: C57BL/6-Tg(Nms-icre)20Ywa/J	Jackson Lab	Cat#027205
Oligonucleotides		
Primers for genotyping and RT-PCR, See Table S1		
Scramble shRNA sequence: CCTAAGGTTAAGTCGCCCTCG	BrainVTA	N/A

(*Continued on next page*)

Continued

REAGENT or RESOURCE	SOURCE	IDENTIFIER
Kcc2 shRNA sequence: GCCATTTCCATGAGTGCAATC	BrainVTA	N/A
Igf2 shRNA sequence: GATCGTGTTACCACCCAAAGA	BrainVTA	N/A
Software and algorithms		
GraphPad Prism 8	GraphPad Software Inc., San Diego, CA, USA	https://www.graphpad.com/scientific-software/prism/
Inper Data Process	Inper	N/A
Neuroscore version 3.3 software	Data Sciences International, New Brighton, MN	N/A
R studio	N/A	https://www.rstudio.com/
Clocklab	Actimetrics, Evanston	https://actimetrics.com/products/clocklab/
PyCharm 2020.1.2	JetBrains	https://www.jetbrains.com/pycharm/

RESOURCE AVAILABILITY

Lead contact

Further information and requests for reagents may be directed to, and will be fulfilled by, the lead contact Ying Xu (yingxu@suda.edu.cn).

Materials availability

The B6/JGpt-Vip$^{em1Cin(iCre)}$/Gpt line used in this study is available from the lead contact with a completed Materials Transfer Agreement.

Data and code availability

- All RNA-seq datasets are available from SRA: PRJNA705298.
- The code for wavelet analysis will be available from the lead contact.

EXPERIMENTAL MODEL AND SUBJECT DETAILS

Mouse strain

C57BL/6J mice were purchased from GemPharmatech Co. Ltd and Charles River Laboratories. The Tg(Nms-icre)20Ywa/J mice with C57BL/6 background was purchased from The Jackson Laborotary. The Vip-iCre mice with C57BL/6 background was obtained by inserting a codon optimized Cre recombinase (iCre) into the ATG start site of the *Vip* gene within the BAC transgene technology (Figure S11). All mice were housed in specific pathogen-free animal facility. The animal procedures were approved by the Animal Care and Use Committee of Soochow University. Mice were fed a standard chow diet (ShooBree SPF Mice Diet, 28% protein, 13% fat, 57% carbohydrates).

Cell lines and culture conditions

Rat suprachiasmatic nucleus cell line (SCN 2.2) was purchased from Kerafast (From the laboratory of David J. Earnest, PhD, Texas A&M University), cultured in Dulbecco's modified eagle medium (DMEM)/high glucose containing 10% fetal bovine serum (FBS), 50 U/mL penicillin, and 50 μg/mL streptomycin and maintained in 37°C, 5% CO2 condition.

METHODS DETAILS

Feeding schedule, food intake, and locomotor activity analyses

Six to eight-week-old male C57BL/6J mice were individually housed in cages equipped with running wheels for 2 weeks under the light-dark cycle, with unrestricted access to food and water. After two weeks, food is available only for 4 h per day in zeitgeber time, where ZT0 is lights on and ZT12 is lights off: ZT0-4, ZT2-6, ZT4-8, ZT6-10, ZT8-12, ZT10-14, ZT12-16, ZT14-18, ZT16-20, ZT18-22, ZT20-24, ZT22-2, n = 6 per group. Cages were changed daily during TRF to avoid food leave in the cage. *Ad libitum* control mice (n = 6) underwent the same procedure except for food available at all the time. Food consumptions were

determined daily, and body weights were measured weekly. Wheel running was recorded and analyzed using ClockLab (Actimetrics, Evanston, IL). The onset represents the phase angle difference in minutes between the time of beginning of the activity, while the offset is the phase-angle difference in minutes between the time of the end of activity detected by Clocklab analysis program. The locomotion range is calculated as the average time between onset and offset of locomotor activity for totaling 10 successive days (except for indication) after released to *ad libitum* under constant darkness.

Stereotaxic viral injections

rAAV-VGAT1-Cre-mCherry-WPRE-pA, rAAV-CAG-FLEX-jGCaMP7s-WPRE-SV40 pA, rAAV-Ef1a-mCherry-U6-Loxp-CMV-EGFP-loxp-shRNA (*Kcc2*), rAAV-Ef1a-mCherry-U6-Loxp-CMV-EGFP-loxp-shRNA (Scramble), rAAV-Ef1α-DIO-mCherry-WPRE-pA, rAAV-Ef1α-DIO-hM4D(Gl)-mCherry-WPREs, rAAV-VGAT1-Cre-WPRE-pA, rAAV-CMV-DIO-EGFP-WPRE-pA, rAAV-CMV-DIO-IGF2-2A-EGFP-WPRE-pA, rAAV-Ef1a-mCherry-U6-Loxp-CMV-EGFP-loxp-shRNA (*Igf2*) were obtained from the Brain VTA, Wuhan, China. 2–3 months old animals were initially anesthetized in the isoflurane induction box (2.5% isoflurane) and placed in a stereotaxic head frame during surgery with 1.5% isoflurane. A heating pad was used to prevent hypothermia. 150 nL AAV was bilaterally (unilaterally for Ca^{2+} recording experiment) delivered with a Shanghai Gaoge Industrial 10 μL syringe at the speed of 100 nL/min using an injection pump (ALC-IP, Shanghai Alcott biotech co. ltd). Stereotaxic coordinates for SCN: AP -0.05 mm, ML ± 0.15 mm, DV -5.85 mm.

Ca^{2+} signal recording and signal analysis

200 μm diameter optic fiber was implanted with 5° in SCN immediately after the AAV injection. After 3 weeks, all implanted mice were screened for the rhythmic Ca^{2+} signal using multichannel fiber photometry (Inper). Then, Ca^{2+} signals were recorded from ZT12 (light off) for 84 h in constant darkness in freely moving mice. After entrained in LD for another 3 days, mice were subjected to TRF for 2 weeks and then were released into constant darkness with *ad libitum*. Ca^{2+} signals were again recorded from ZT12 (light off) for another 84 h. The sampling rate is 30 Hz for 470 and 430 nm LED with power of 15–20 μw. The signal was recorded 35S every 10 min to prevent the phototoxicity to the SCN neurons. The 430 nm signal is used to eliminate the noise caused by mouse movement or environmental interruption. Signals were then extracted by Inper Data Process software and the raw data was normalized to 0–100 to counteract the difference of fluorescence strength result from the mild deviation of optic fiber location and virus expression. We then use PyCharm software to do wavelet analysis and calculated time-series signal power with different frequency. The Ca^{2+} intensity was calculated in 1-h temporal resolution. Because there is a two-week interval before and after TRF that led to baseline intensity changes, we normalized the Ca^{2+} intensity of ZT23-4 TRF window (ZT23-CT3, CT23-CT27, CT47-CT51) and ZT7-12 TRF window (CT7-CT11, CT31-CT35, CT55-CT59) by 14 h period of Ca^{2+} active phase in the corresponding day (ZT23-CT13, CT23-CT37 and CT47-CT61). The relative intensity changes in each day in the same mice were calculated and compared. All data were subtracted the mean trend from the raw data and removed the damping effects.

SCN lesions

Bilateral SCN lesions were performed stereotaxically in 2-month-old C57BL/6J mice under isoflurane anesthesia. A heating pad was used to prevent hypothermia. First, a small hole was drilled on the surface of the skull after leveling. A platinum-iridium alloy electrode (0.15-mm diameter, Kedou Brain-Computer Technology Co., Ltd.) coated with polyimide except for the tip (0.2 mm in length) was inserted bilaterally into the SCN (Stereotaxic coordinates for SCN lesion: AP -0.05 mm, ML ± 0.15 mm, DV -5.85 mm). The SCN was then lesioned by 0.4 mA current for 40 s with a Ugo Basile lesion making device (model 53,500). The electrode was left for 1 min before withdrawing from the brain. After the SCN lesion, wheel-running activities were recorded under LD cycles for at least 1 week to confirm the loss of circadian rhythms. The sham lesioned mice underwent the same operation, but the electrode was inserted to a 5.4 mm depth from the skull surface, and no current was passed through the electrode.

Sleep-wake monitoring and analysis

2-month-old mice were surgically implanted with HD-X02 biotelemetry transmitters (Data Sciences International [DSI], New Brighton, MN) according to the manufacturer's protocol (DSI EET Device Surgery Manual). Mice were deeply anesthetized with isoflurane (2.5% induction, 1.5% maintenance) and immobilized in a stereotaxic apparatus. After exposing and cleaning the skull, two stainless steel screws were

inserted above the dura membrane as cortical electrodes. The other pair of screws were inserted into the cervical trapezius muscles to record EMG. The electrodes above the skull were fixed with dental acrylic, and the transmitter was pocked under the back. Mice were allowed to recover for at least 7 days before starting the experiment. The EEG and EMG data were collected for 3 days from CT0 to CT72 for both before TRF and after ZT0-4 TRF.

EEG (filtered by 0–30 Hz) and EMG signal sampled at 500 Hz were analyzed using the Neuroscore version 3.3 software (Data Sciences International [DSI], New Brighton, MN). The delta (0.5–4 Hz) (NREM), alpha (8–12 Hz) (wake) and theta (4–8 Hz) (REM) power percentage was assessed by calculating the power (FFT) per 10-s epoch and the average power per hour for every sleep epoch and finally were expressed hourly and in 72 h.

GSK1904529A, chromeceptin administration and osmotic pump implantation

The GSK1904529A and Chromeceptin were diluted in 5% DMSO, 20% PEG300 and 75% saline with a final concentration of 0.05 and 0.15 mM. The 5.5 mm stainless tube with 300 mm diameter was connected to a 100 mL osmotic pump through a rubber hose and then filled with DMSO/PEG300 (as control), GSK1904529A and Chromeceptin solution. Mice were initially anaesthetized in the isoflurane induction box (2.5% isoflurane) and placed in a stereotaxic head frame during surgery with 1.5% isoflurane. After the exposure of the brain bregma site, a stainless tube was then implanted with 3° and finally fixed above the SCN with dental cement. The stereotaxic coordinates for tube: AP -0.05 mm, ML + 0.30 mm, DV -5.60 mm. Then all mice were recovered to the wheel-running cage after the surgery. A heating pad was used to prevent hypothermia during surgery.

SCN 2.2 culture and IGF2 administration

Rat SCN 2.2 cells were cultured in Dulbecco's modified eagle medium (DMEM)/high glucose containing 10% fetal bovine serum (FBS), 50 U/mL penicillin, and 50 μg/mL streptomycin and maintained in 37°C, 5% CO_2 condition. Recombinant human IGF-2 was dissolved in PBS contain 0.1% BSA with concentration of 100 mg/mL and stored in −80°C. Plate SCN2.2 cells to be 80–90% confluent and IGF2 was added to culture medium with final concentration of 5 ng/mL (IGF2-L), 50 ng/mL (IGF2-M) and 500 ng/mL (IGF2-H). PBS contain 0.1% BSA without IGF2 was added in the control groups. After 48 h, the SCN2.2 RNA was extracted by Trizol Reagent (ThermoFisher).

Immunofluorescence for SCN slice

After anesthesia by pelltobarbitalum natricum, mice were perfused with PBS and 4% paraformaldehyde. Then brains were collected, fixed in 4% paraformaldehyde overnight at 4°C. Coronal sections (30 μm thick) were cut using a vibratome (Leica VT1000s). Sections with SCN (the middle part) were used for immunofluorescence. Free-floating sections were washed in PBS, incubated for 30 min in blocking buffer (1% BSA and 0.3% Triton X-100 in PBS) and incubated overnight at 4°C with anti-KCC2 (Proteintech) primary antibody diluted 1:500 in the blocking buffer. Sections were then washed in PBS and incubated for 1 h at room temperature with Alexa Fluor 488 Donkey anti-rabbit IgG (ThermoFisher) or Alexa Fluor 594 Goat anti-rabbit IgG (ThermoFisher) diluted 1:500 in blocking buffer. Sections were again washed and incubated with DAPI (1:10,000 in PBS) for 5 min when needed. After washed with PBS, sections were mounted on adhesion microscope slides (19017, Citotest) and air-dried in darkness. Slides were cover-slipped with 75% glycerin and sealed with nail polish. Fluorescence-immunolabeled images were acquired using an Olympus fluorescence microscope.

RNA-seq and differently expressed genes analyses

After cervical dislocation, the mice brain was placed in ice-cold PBS, and the SCN samples were collected with a 1.5 mm tissue punch (Integra Miltex) in 3 min, and SCN samples were stored in liquid nitrogen immediately. The total RNA of SCN was extracted with Trizol Reagent (ThermoFisher), and the GlycoBlue was added during RNA extracted to visualize the RNA product. For RNA-seq, the quality of the total RNA was determined using an Agilent 2200 TapeStation, and RNA-seq was performed on an Illumina NovaSeq 6000 platform with PE 150-bp reads at the Genewiz, Suzhou, China. Paired-end clean reads were aligned to the NCBI reference genome mm10 using Hisat2 (v2.0.5) and assembled using Stringtie (v1.3.3). Cuffdiff v1.3.0 was used to calculate FPKMs for coding genes in each sample.

To identify genes with a daily rhythmic expression from the gene expression data in different experimental groups, the Jonckheere-Terpstra-Kendall (JTK) algorithm in R studio was used. A permutation-based p-value (ADJ.P) of less than or equal to 0.05 was considered significant for all array sets. The optimal phase (LAG), amplitude (AMP), and period (PER) estimates for each transcript of oscillating genes were extracted from the JTK algorithm. Cuffdiff v2.2.1 provides statistical routines for determining differential expression in digital transcript or gene expression datasets using a negative binomial distribution model. Genes with corrected p-value less than 0.05 and the fold change greater than or equal to 2 were assigned as significantly differentially expressed genes (DE-Gs). Finally, the rhythmic change genes and DE-Gs are defined as differently expressed genes.

PCA and Gene Ontology analysis

RNA-seq raw data were first subjected to Bartlett's Test of Sphericity to validate its adequacy for PCA ($p < 0.0001$), after which correlation-based PCA was implemented in R studio using factoextra and FactoMineR packages. Broken Stick model was used to determine the number of retainable PCs and we retained the first two PCs, which collectively explained 73.1% of the variance in different groups. Specifically, we aimed to identify the most relevant pathways to the beginning of the light period behavior, the unsuitable pathways or enrichment annotations such as colorectal cancer, HIV infection, tuberculosis were removed from the datasets. Gene Ontology and pathway analysis were performed by DAVID (https://david.ncifcrf.gov/home.jsp) to significantly enriched GO terms and biological process at p values <0.01 (Bonferroni) compared with the whole-transcriptome background.

RT-PCR

The SCN total RNA was extracted with Trizol Reagent (ThermoFisher). For the quantitative real-time RT-PCR, the RNA concentration was determined by a NanoDrop (Thermo), and the cDNA was synthesized using a PrimeScript RT Reagent Kit (Takara). Quantitative real-time RT-PCR was performed using SYBR Premix Ex Taq with StepOne Plus (Applied Biosystems). The relative levels of *Igf2*, *Kcc2*, *Bmal1*, *Per1*, *Per2*, *Avp* and *Pk2* were normalized to *Gapdh*. Primer information for RT-PCR is included in the Table S1.

QUANTIFICATION AND STATISTICAL ANALYSIS

All the statistical analyses were performed using Student's *t*-tests or two-way ANOVAs using GraphPad Prism 8 (GraphPad Software Inc., San Diego, CA, USA). A $p < 0.05$ was considered statistically significant (*$p < 0.05$, **$p < 0.01$, and ***$p < 0.001$).